TensorAlloy: an automatic atomistic neural network program for alloys

Xin Chen[a], Xing-Yu Gao[a], Ya-Fan Zhao[b,a], De-Ye Lin[b,a,*], Wei-Dong Chu[a], Hai-Feng Song[a,b,*]

[a]*Institute of Applied Physics and Computational Mathematics, Beijing 100088, China*
[b]*CAEP Software Center for High Performance Numerical Simulation, Beijing 100088, China*

Abstract

Atomistic modeling is important for studying physical and chemical properties of materials. Recently, machine learning interaction potentials have gained much more attentions as they can provide density functional theory level predictions within negligible time. The symmetry function descriptor based atomistic neural network is the most widely used model for modeling alloys. To precisely describe complex potential energy surfaces, integrating advanced metrics, such as force or virial stress, into training can be of great help. In this work, we propose a virtual-atom approach to model the total energy of symmetry function descriptors based atomistic neural network. Our approach creates the computation graph directly from atomic positions. Thus, the derivations of forces and virial can be handled by TensorFlow automatically and efficiently. The virtual atom approach with AutoGrad within TensorFlow allows for efficient training to not just energies and forces, but also virial stress. This new approach is implemented in our open-source program TensorAlloy, which supports constructing machine learning interaction potentials for both *molecules* and *solids*. The QM7 and SNAP/Ni-Mo datasets are used to demostrate the performances of our program.

Keywords: Machine Learning; Alloy; Materials Modeling; Computational Physics; Neural Network

PROGRAM SUMMARY

Program Title: TensorAlloy
Licensing provisions(please choose one): LGPL
Programming language: Python 3.7
Supplementary material:
Journal reference of previous version:
Does the new version supersede the previous version?:
Reasons for the new version:
*Summary of revisions:**
Nature of problem:
Modeling interatomic interactions with the symmetry function descriptor based atomistic neural networks.
Solution method:
The TensorAlloy program is built upon TensorFlow and the virtual-atom approach. TensorAlloy can build direct computation graph from atomic positions to total energy. Atomic forces and virial stress tensors are

---

handled by TensorFlow automatically and efficiently.

Additional comments including Restrictions and Unusual features

This program needs TensorFlow 1.13.*. Neither newer or older TensorFlow is supported.

1. Introduction

Atomistic simulations (*ab initio* calculation, classic molecular dynamics simulation (MD), etc) are powerful tools for studying physical and chemical properties of materials. To obtain reliable simulation results, atomistic interactions must be properly described. The very accurate *ab initio* and quantum chemical methods have gain significant improvements over the past decades but their applicabilities are restricted by computation expenses. Physical model based empirical potentials, such as the embedded-atom method[1, 2, 3, 4, 5] or its variants (modified embedded-atom method[5, 6, 7, 8], angular-dependent interaction potential[9, 10, 11], etc), are much more popular for long-time simulation because of their reasonable accuraty and acceptable costs. However, designing empirical potentials and optimizing parameters for alloys are still challenging tasks[5, 10, 12].

In the past few years, machine learning (ML) has become one of the most influential topic in almost all fields of science. A lot of effort has been made by various physicists to explore the possiblity of using ML models —instead of traditional empirical potentials —to describe atomistic interactions during MD simulations[13, 14, 15, 12, 16, 17, 18]. ML potentials are much easier to design and optimize. With sufficient training data, ML models can achieve similar or even better performances compared with density functional theory. The symmetry function based atomistic neural network (ANN) model, first proposed by Parinello and Behler in 2007[19, 20, 21, 22, 23], is still the most widely used method for *solids* and its effectness and accuracy has been proven by several works[24, 25, 26, 27]. Until now, various ML implementations[28, 17, 18] have been published by researchers. The Amp[28] package, developed by Peterson's group, is the first open-source framework that implements the symmetry function descriptor. Amp can be used to learn interaction potentials for both *molecules* and *solids* and it has successfully powered quite a few researches since 2016[29, 30]. TensorMol[18] and its sucessor TorchANI[17] are also symmetry function based ANN programs but they mainly focus on *molecules*.

In order to precisely model atomistic interactions, both total energy and atomic forces are necessary. For *solids*, the virial stress tensor is also an essential metric. However, integrating force and stress into the loss function is not an easy task. The machine learning approaches favor vectorizable operations but the calculations of atomic descriptors are typically complicated so that many traditional ML packages (Amp, kCON, etc) choose to pre-compute descriptors and only build computation graph from descriptors to total energy. This traditional approach can significantly reduce technical difficulty and works very well if only total energy is considered in the loss function. But to fit atomic forces, numerous codes must be written manually, such as the derivation of descriptors with respect to positions. Although the derivation is theoretically clear, the implementation is challenging and the efficiency can not be guaranteed.

Recently, machine learning platforms (TensorFlow[31], PyTorch[32], MXNet[33], etc) have gain significant developments. These modern machine learning frameworks can fully take advantage of GPUs for acceleration. The automatic differentiation capability brings a new route for devloping ML models capable of predicting energy, force and stress as we may 'let' ML platforms to handle the calculations of force and stress because these metrics can be derived from

2

positions and total energy directly. To achieve this, a direct computation graph from positions to total energy must be built. Thus, the problem becomes: how to design such route?

In this work, we propose a new TensorFlow-dependent apporach (the virtual atom approach, VAP) to model the total energy expression of the symmetry function descriptor based neural network. Our apporach can move the entry of the computation graph from atomic descriptors back to the raw atomic positions. Thus, calculating the derivatives of total energy with respect to atomic positons (force) or lattice tensor (virial) can be handled by TensorFlow directly and automatically. Hence, the technical barrier of training ANNs with atomic forces and (especially) virial stress becomes completely neglectable.

This paper is organized as follows. Section 2 introduces the theory of the symmetry function descriptor and the ANN framework. Section 3 describes the virtual atom approach and the modified ANN model used by TensorAlloy. Section 4 demostrates the performances of TensorAlloy on two public datasets. The appendix 5 gives derivation and implementation details of key routines of VAP.

2. Theory

In the atomistic neural network (**ANN**) framework, the total energy, E^{total}, of a structure with N atoms, can be expressed as the sum of all atomic energies:

$$E^{total} = \sum_i^N E_i \tag{1}$$

where E_i, the energy of atom i, is the output of the neural network $\mathbf{NN}_{el}$ for element el:

$$E_i = \mathbf{NN}_{el}(\mathbf{G}_i) \tag{2}$$

Here $\mathbf{G}_i$ is a vector representing atomic descriptors of atom i. $\mathbf{G}_i$ typically only depends on local environment of atom i, i.e. its neighbors:

$$\mathbf{G}_i = F_G\left(\left\{r_{ij\mathbf{n}}, |r_{ij\mathbf{n}}| < r_c\right\}\right) \tag{3}$$

where F_G is a specifc feature function, r_c is the cutoff radius and $r_{ij\mathbf{n}}$ is the interatomic distance considering the periodic boundary conditions:

$$r_{ij\mathbf{n}} = \|\mathbf{r}_i^{(0)} - \mathbf{r}_j^{(0)} + \mathbf{n}^T\mathbf{h}\| \tag{4}$$

where $\mathbf{r}_i^{(0)}$ and $\mathbf{r}_j^{(0)}$ denote positions of atoms i and j in the primitive cell, $\mathbf{n}$ is a column vector specifying the cell shifts along (X, Y, Z) directions

$$\mathbf{n} = \begin{pmatrix} n_x \\ n_y \\ n_z \end{pmatrix} \tag{5}$$

and $\mathbf{h}$ is the **row-major** 3×3 lattice tensor:

$$\mathbf{h} = \begin{pmatrix} h_{xx} & h_{xy} & h_{xz} \\ h_{yx} & h_{yy} & h_{yz} \\ h_{zx} & h_{zy} & h_{zz} \end{pmatrix} \tag{6}$$

3

There are many choices of F_G. The symmetry function descriptor, proposed by Parinello and Behler in 2007[19], is currently the most widely used atomic descriptor. The symmetry function descriptor consists of two types of functions: the radial symmetry function $\mathbf{G}^{(2)}$ and the angular symmetry function $\mathbf{G}^{(4)}$:

$$\mathbf{G}_i^{(2)}(\eta, \omega) = \sum_{j \neq i} \sum_{\mathbf{n}} g_2(\eta, i, j, \omega) \tag{7}$$

$$\mathbf{G}_i^{(4)}(\beta, \gamma, \zeta) = 2^{1-\zeta} \sum_{j,k \neq j, k \neq i} \sum_{\mathbf{n}_1} \sum_{\mathbf{n}_2} \sum_{\mathbf{n}_3} g_4(\beta, \gamma, \zeta, i, j, k, \mathbf{n}_1, \mathbf{n}_2, \mathbf{n}_3) \tag{8}$$

$$g_2(\eta, i, j, \omega) = \exp\left\{-\frac{\eta(r_{ij\mathbf{n}} - \omega)^2}{r_c^2}\right\} \cdot f_c(r_{ij\mathbf{n}}) \tag{9}$$

$$g_4(\beta, \gamma, \zeta, i, j, k, \mathbf{n}_1, \mathbf{n}_2, \mathbf{n}_3) = (1 + \gamma \cos\theta)^\zeta \exp\left\{-\frac{\beta(r_{ij\mathbf{n}_1}^2 + r_{ik\mathbf{n}_2}^2 + r_{jk\mathbf{n}_3}^2)}{r_c^2}\right\}$$
$$\times f_c(r_{ij\mathbf{n}_1}) f_c(r_{ik\mathbf{n}_2}) f_c(r_{jk\mathbf{n}_3}) \tag{10}$$

where η, ω, β, γ and ζ are empirically chosen parameters, $f_c(r)$ is a cutoff (damping) function and its original form is:

$$f_c(r) = \begin{cases} 0 & r > r_c \\ \frac{1}{2} + \frac{1}{2}\cos(r/r_c \cdot \pi) & r \leq r_c \end{cases} \tag{11}$$

and r_c is the cutoff radius. Equation (11) can be further transformed to a vectorized expression:

$$f_c(r) = \frac{1}{2}\left(1 + \cos\left[\min(\frac{r}{r_c}, 1)\pi\right]\right) \tag{12}$$

and $\cos\theta$ also has a vectorized form:

$$\cos\theta = \frac{r_{ij\mathbf{n}_1}^2 + r_{ik\mathbf{n}_2}^2 - r_{jk\mathbf{n}_3}^2}{2r_{ij\mathbf{n}_1} \cdot r_{ik\mathbf{n}_2}} \tag{13}$$

The summations in Equation 7 and 8 should go over all neighbors within r_c. For an atom i, $\mathbf{G}_i$ is a vector. For the entire structure, its overall $\mathbf{G}$ is a matrix with row i represents the atomic descriptors of atom i and column j corresponds to a specifc (η, ω) pair or (β, γ, ζ) combination.

Analytical atomic forces can be obtained directly by computing the first-order derivative of E^{total} with respect to $\mathbf{r}_a^{(0)}$ where a is an index:

$$f_a = -\frac{\partial E^{total}}{\partial \mathbf{r}_a^{(0)}} \tag{14}$$

According to the chain rule, we can expand Equation 14:

$$\frac{\partial E^{total}}{\partial \mathbf{r}_a^{(0)}} = \sum_i^N \frac{\partial \mathbf{NN}_{el}(\mathbf{G}_i)}{\partial \mathbf{r}_a^{(0)}}$$
$$= \sum_i^N \sum_l^{N_G} \frac{\partial \mathbf{NN}_{el}(\mathbf{G}_i)}{\partial G_{il}} \cdot \frac{\partial G_{il}}{\partial \mathbf{r}_a^{(0)}} \tag{15}$$

4

and

$$\frac{\partial G_{il}^{(2)}}{\partial \mathbf{r}_a^{(0)}} = \sum_{j \neq i} \sum_{\mathbf{n}} \frac{\partial g_2}{\partial r_{ij\mathbf{n}}} \cdot \frac{\partial r_{ij\mathbf{n}}}{\partial r_k^0} \tag{16}$$

$$\frac{\partial G_{il}^{(4)}}{\partial \mathbf{r}_a^{(0)}} = 2^{1-\zeta} \sum_{j,k \neq j, k \neq i} \sum_{\mathbf{n_1}} \sum_{\mathbf{n_2}} \sum_{\mathbf{n_3}} \left(\frac{\partial g_4}{\partial r_{ij\mathbf{n_1}}} \frac{\partial r_{ij\mathbf{n_1}}}{\partial \mathbf{r}_a^{(0)}} + \frac{\partial g_4}{\partial r_{ik\mathbf{n_2}}} \frac{\partial r_{ik\mathbf{n_2}}}{\partial \mathbf{r}_a^{(0)}} + \frac{\partial g_4}{\partial r_{jk\mathbf{n_3}}} \frac{\partial r_{jk\mathbf{n_3}}}{\partial \mathbf{r}_a^{(0)}} \right) \tag{17}$$

The derivations are theoretically straightforward but their implementations are challenging [28]. Later we will provide an automatic approach to address this problem.

The 3×3 virial tensor ϵ is an important metric to describe solids under deformation or external pressure. For arbitrary many-body interaction potentials, ϵ can be calculated with the following equation [34]:

$$\epsilon = \left(-\sum_{i=1}^{N} \mathbf{r}_i^{(0)} \otimes f_i - \sum_{\mathbf{n}} \mathbf{h}^T \mathbf{n} \otimes \sum_{i=1}^{N} F'_{i\mathbf{n}} \right)^T \tag{18}$$

where $\otimes$ indicates tensor product, f_i is the total force acting on atom i and $F'_{i\mathbf{n}}$ is the partial force. Until now, most machine learning force-field models focus on fitting total energy and atomic forces, very few of them[35, 36, 37] had attempted to include stress in their loss functions. The current expression of Equation 18 is not very compatible with NN or other ML potentials since the partial forces are difficult to compute with vectorized operations. However, we find an "equivalent" form of Equation 18:

$$\epsilon = -F^T R + \left(\frac{\partial E^{total}}{\partial \mathbf{h}} \right)^T \mathbf{h} \tag{19}$$

where R is the $N \times 3$ positions matrix and F is the corresponding total forces matrix. This new form can be easily implemented within TensorFlow. The detailed derivation is given in the appendix(A).

3. Method

In this section we will describe the architecture of TensorAlloy and the core algorithm: the virtual atom approach (VAP). The most noticable feature of the TensorAlloy program is that the calculation of symmetry function descriptors is automatically handled by the **AutoGrad**[31] routine of TensorFlow because we successfully find a route (VAP) to build the direct computation graph from atomic positions to total energy.

The Ni-Mo binary alloy system will be used as the example to show our algorithms. The original dataset (SNAP) is published by Shyue Ping Ong[12]. For simplicity, only radial symmetry function related algorithms are visualized in the figures. Python3.7 implementations of key algorithms and functions are given in the appendix.

3.1. Overview

Fig 1 shows the overview of TensorAlloy and the virtual-atom approach. TensorAlloy has two phases: the training phase (**1**) and the prediction phase (**2**). These two phases share many common requirements, but they also have their own concerns.

For the training phase, in order to make TensorAlloy a general-purpose and efficient machine learning potential training program, there are some key technical requirements:

1. Stoichiometry-free: the training dataset should not have any stoichiometry restriction. Any type of *solid* or *molecule* is acceptable. A universal approach of expressing different structures in a single reference system may be necessary.

2. Mini-batch training: mini-batch based stochastic training is currently the most efficient way to train neural networks on large datasets. However, batch training requires *vectorized* and *aligned* expressions. Here *aligned* means feature arrays of structures of different stoichiometries share the same shape.

3. Cache: some intermediate arrays may be pre-computed and stored in cache files. During training, these values can be loaded from cache directly, thus saving significantly amount of resources.

In the prediction phase, the situation is a bit different. The stoichiometry of the target structure or molecule may not be included in the training dataset and it can vary significantly. TensorAlloy must be capable of handling such (extreme) situations. For example, the trained Ni-Mo shall be applicable to any any $Ni_x Mo_y$ structure while x and y can be either as large as 100000 or as small as 0.

Besides, we also want our TensorAlloy program have an *independent* and *user-friendly* prediction phase. Users can just focus on the integration of machine learning potentials with their own researches.

VAP plays a central role in handling all the technical challenge as it ***provides a way to describe structures of various sizes and stoichiometries in unified and vectorized forms***. In the following sections, we will gradually discuss the details of this approach.
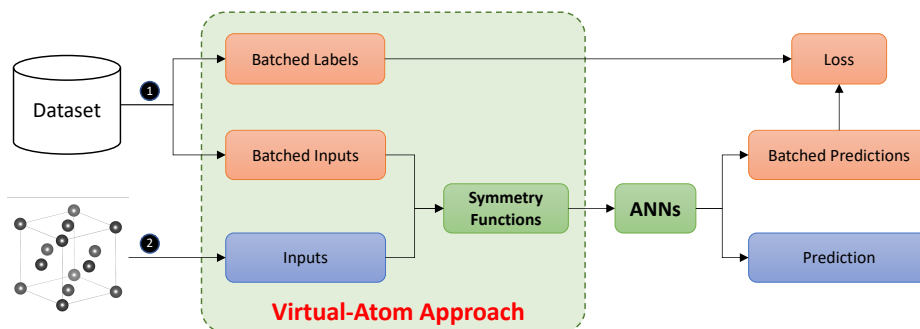

Figure 1: The general design of TensorAlloy. **(1)** demonstrates the training phase while **(2)** represents the prediction phase.

3.2. Preparation

Fig 2 shows the preparation stage of VAP. The cutoff radius r_{cut} must be fixed. This stage has two major steps. The first step is to build the global symbol list (GSL), which acts as the universal reference system. A virtual atom is inserted at the very first position of GSL. To build GSL, all $\{N_{el}^{max}\}$ must be pre-determined where N_{el}^{max} is the maximum appearances of element *el* in any structure. $N_{element}$ represents the number of unique chemical elements in the dataset. Then, N^{vap}, the dimension of GSL, can be determined:

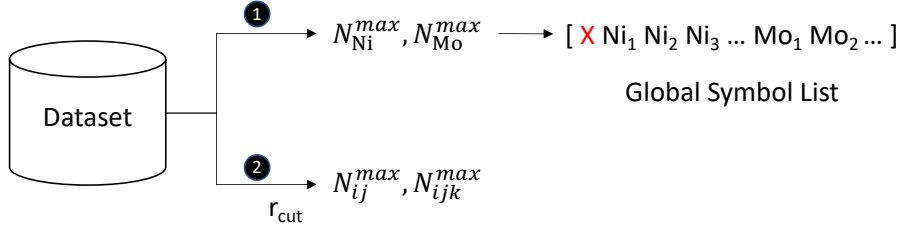$$N^{vap} = 1 + \sum_{el} N_{el}^{max} \qquad (20)$$

6

Figure 2: The initialization step. **(1)** describes the detections of $N_{\mathrm{Ni}}^{\max}$, $N_{\mathrm{Ni}}^{\max}$ and the global symbol list (GSL). The red 'X' represents the inserted virtual atom. **(2)** shows the detections of $N_{ij}^{\max}$ and $N_{ijk}^{\max}$ given r_{cut}.

For the Ni-Mo dataset, $el \in [\mathrm{Ni}, \mathrm{Mo}]$ and $N_{\mathrm{element}} = 2$. Table 1 gives some examples of the GSL mapping. 'X' denotes the inserted virtual atom and $\mathrm{Ni}_{108(54)}$ means the first 54 Ni atoms are mapped from the local stoichiometry. In the training phase, all $N_{\mathrm{el}}^{\max}$ are fixed. In the prediction phase, $N_{\mathrm{el}}^{\max}$ shall be determined dynamically. One should note that the minimum value of $N_{\mathrm{el}}^{\max}$ should be 1 due to technical reason (so that the computation graph of TensorFlow can be properly executed). The codes to get $N_{\mathrm{el}}^{\max}$ and GSL are given in Appendix(C). With GSL setup, atomic positions and forces can be transformed as well. Appendix(D) gives the implementation of the virtual-atom mapping mechanism.

	Stoichiometry (Local)	$N_{\mathrm{Ni}}^{\max}$	$N_{\mathrm{Mo}}^{\max}$	N^{vap}	Stoichiometry (GSL)
	Ni_{54}				$\mathrm{XNi}_{108(54)}\mathrm{Mo}_{176(0)}$
Training	$\mathrm{Ni}_{54}\mathrm{Mo}_{12}$	108	176	285	$\mathrm{XNi}_{108(54)}\mathrm{Mo}_{176(12)}$
	Mo_{12}				$\mathrm{XNi}_{108(0)}\mathrm{Mo}_{176(12)}$
	Ni_{54}	54	1	56	$\mathrm{XNi}_{54(54)}\mathrm{Mo}_{1(0)}$
Prediction	$\mathrm{Ni}_{54}\mathrm{Mo}_{12}$	54	12	68	$\mathrm{XNi}_{54(54)}\mathrm{Mo}_{12(12)}$
	Mo_{12}	1	12	14	$\mathrm{XNi}_{1(0)}\mathrm{Mo}_{12(12)}$

Table 1: The mappings of local stoichiometries to their GSL forms, taking examples of the SNAP/Ni-Mo dataset.

Then we can determine another two key constants: $N_{ij}^{\max}$ and $N_{ijk}^{\max}$. Here $N_{ij}^{\max}$ represents the maximum number of atom-atom pairs in arbitrary structure and the subscript 'ijk' denotes triples (or three-atoms) interactions. $N_{ij}^{\max}$ and $N_{ijk}^{\max}$ only depend on r_{cut} and the associated codes are given in Appendix(B). Table 2 summarizes $N_{ij}^{\max}$ and $N_{ijk}^{\max}$ at different r_{cut} of the two demo datasets: QM7 and Ni-Mo (SNAP).

Dataset	$r_{cut}(\text{Å})$	$N_{ij}^{\max}$	$N_{ijk}^{\max}$
QM7	6.5	506	5313
SNAP/Ni-Mo	4.6	7200	176400
	6.0	12384	526320
	6.5	16284	965338

Table 2: $N_{ij}^{\max}$ and $N_{ijk}^{\max}$ of SNAP/Ni-Mo and QM7 at different r_{cut}.

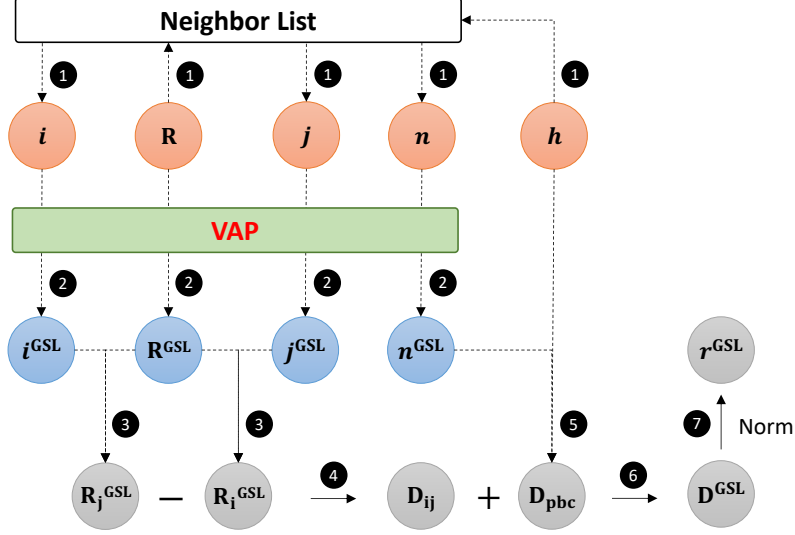Figure 3: The pseudo computation graph with execution orders for calculating interatomic distances **r** from atomic positions **R** and lattice tensor **h**.

3.3. Interatomic distances

Both the radial (Equation 9) and the angular (Equation 10) symmetry functions depends on interatomic distances only. In order to compute the descriptors, local atomic positions should be transformed to interatomic distances first. Fig 3 demonstrates the pseudo graph of $\mathbf{R} \rightarrow \mathbf{r}^{GSL}$ for radial symmetry function descriptors:

1. Find all (i,j) neighbor pairs using the routine *neighbor_list* implemented in ASE[38]. **R** represents local atomic positions, **h** is the lattice tensor. **i** and **j** are vectors of length N_{ij} and **n** is the $N_{ij} \times 3$ periodic boundary shift matrix. In the training phase $N_{ij} \leq N_{ij}^{\max}$; in the prediction phase, $N_{ij}^{\max}$ is exactly equal to N_{ij}.

2. Transform and expand local **R**, **i**, **j** and **n** to their corresponding GSL arrays. These GSL arrays can be cached for training. The transformations of **i**, **j** and **n** are straightforward: just appending $N_{ij}^{\max} - N_{ij}$ trailing zeros. Fig 4 shows the mapping of $\mathbf{R} \rightarrow \mathbf{R}^{GSL}$ taking the example of Ni_3Mo_2.

3. Broadcast $\mathbf{R}^{GSL}$ to $\mathbf{R}_i^{GSL}$ and $\mathbf{R}_j^{GSL}$ with $\mathbf{i}^{GSL}$ and $\mathbf{j}^{GSL}$ respectively.

4. Compute the displacement vectors in the original cell: $\mathbf{D}_{ij} = \mathbf{j}^{GSL} - \mathbf{i}^{GSL}$

5. Compute the periodic displacements: $\mathbf{D}_{pbc} = \mathbf{n}^{GSL}\mathbf{h}$

6. Compute the overall GSL displacements: $\mathbf{D}^{GSL} = \mathbf{D}_{pbc} + \mathbf{D}_{ij}$

7. Compute the interatomic distances $\mathbf{r}^{GSL}$ by calculating the 2-norm of each row of matrix $\mathbf{D}^{GSL}$.

Steps 1-2 are implemented in the function *get_g2_map* in Appendix(E). Steps 3-7 are implemented in the method *get_rij* of class *SymmetryFunction* in Appendix(G).
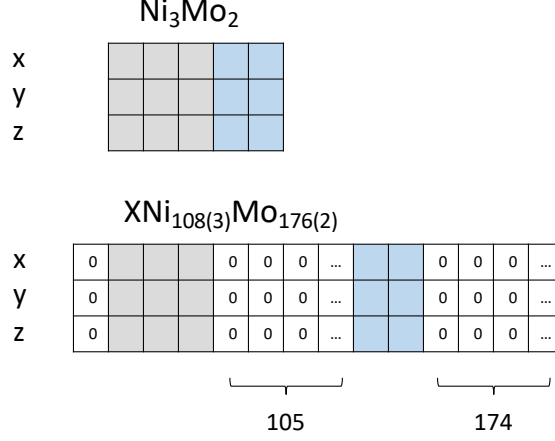
8

Figure 4: The transformation of local $\mathbf{R}$ of Ni_3Mo_2 to $\mathbf{R}^{GSL}$ of $XNi_{108(3)}Mo_{176(2)}$.

3.4. Radial descriptors

Now we can start computing radial symmetry descriptors $\mathbf{G}^{(2)}$ from $\mathbf{r}^{GSL}$. For simplicity, we will use the prediction phase to demonstrate this final section.

Suppose we have N_τ different (η, ω) pairs for Equation 7 and $(\eta, \omega)_\tau (0 \leq \tau < N_\tau)$ represents the $(\tau + 1)$-th pair. In the prediction phase, $\mathbf{r}^{GSL}$ should be a vector of length N_{ij}^{max} and the desired output $\mathbf{G}^{(2)}$ will be a matrix of shape $[N^{vap}, (N_{element})^2 \cdot N_\tau]$, as shown in Fig 6d:

1. The total number of rows is N^{vap} (Equation 20) and each row represents the complete radial symmetry function descriptors of an atom. The first row always corresponds to the inserted virtual atom.

2. The total number of columns is $N_{element} \cdot N_{element} \cdot N_\tau$. Here $N_{element} \cdot N_{element}$ indicates the number of element-element interaction types and each interaction is described by N_τ feature values. For the Ni-Mo dataset, there should be four unqiue interaction types: Ni-Ni, Ni-Mo, Mo-Mo and Mo-Ni.

Assume v is a vector of length N_v, we can define an integer matrix f_v^S for mapping v to a new array g of shape S satisfying the following conditions:

$$g(p) = \sum_{\tau=0}^{\tau < N_v} c_\tau(p) \cdot v(\tau) \tag{21}$$

$$c_\tau(p) = \begin{cases} 1 & f^S{}_v(\tau) = p \\ 0 & \text{else} \end{cases} \tag{22}$$

where p is a coordinate vector. The matrix f_v^S shall have N_v rows and N_S columns where N_S represents the dimension of g. Fig 5 visualizes this f_v^S mapping scheme. This f_v^S mapping plays a key role in transforming $\mathbf{r}^{GSL}$ to $\mathbf{G}^{(2)}$.
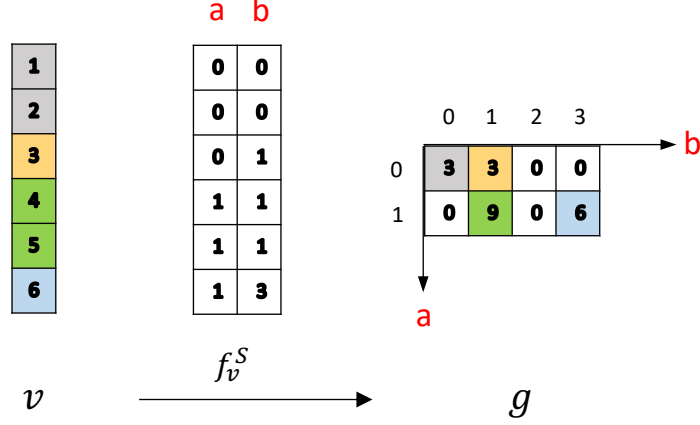
9

Figure 5: The visualization of the mapping f_v^S. In this example $S = [2, 4]$ and p can be any (i, j) if $0 \leq i < 2$ and $0 \leq j < 4$.

Fig 6 demonstrates the calculation of $\mathbf{G}^{(2)}((\eta, \omega)_\tau)$ from $\mathbf{r}^{\text{GSL}}$. $\mathbf{G}^{(2)}((\eta, \omega)_\tau)$ is the partial descriptors contributed by the τ-th (η, ω) combination. The overall $\mathbf{G}^{(2)}$ is just the sum of all partial contributions:

$$\mathbf{G}^{(2)} = \sum_{\tau=0}^{\tau<N_\tau} \mathbf{G}^{(2)}((\eta, \omega)_\tau) \tag{23}$$

This calculation can be easily implemented with a *For* loop. For each τ, there will be three major steps:

1. The first step is applying Equation 9 on $\mathbf{r}^{\text{GSL}}$ with the given τ-th (η, ω) pair to obtain $g_2^{\text{GSL}}((\eta, \omega)_\tau)$. $g_2^{\text{GSL}}((\eta, \omega)_\tau)$ is a vector of length $N_{ij}^{\max}$ and its last $(N_{ij}^{\max} - N_{ij})$ components are dummy values.

2. The second step is generating the mapping $f_{g,\tau}^S$. In the Ni-Mo case, $S = [285, 4N_\tau]$. $f_{g,\tau}^S$ is a matrix of shape $[N_{ij}^{\max}, 2]$ and $f_{g,\tau}^S$ is constructed from the base mapping array f_g^S by adding τ to its second column. f_g^S is also a $N_{ij}^{\max} \times 2$ matrix. f_g^S stores fundamental properties of $\mathbf{r}^{\text{GSL}}$: the center atom (e.g. Ni_1) and type (e.g. Ni-Mo) of each atom-atom interaction:

   a. Its first column is directly copied i^{GSL}, representing the GSL indices of the center atoms.

   b. The values of its second column are multiples of N_τ indicating the offsets, or horizontal positions in $\mathbf{G}^{(2)}$. These values are obtained by multiplying N_τ with the type indices of $\mathbf{r}^{\text{GSL}}$. For example, the Ni-Mo dataset has two unique elements: Ni, Mo. Hence, there will be four types of interactions: Mo-Mo (0), Mo-Ni (1), Ni-Ni (2) and Ni-Mo (3). Then for each value (atom-atom interaction) of $\mathbf{r}^{\text{GSL}}$, its type index can be determined with $\mathbf{i}^{\text{GSL}}$ and $\mathbf{j}^{\text{GSL}}$ based on the pre-built GSL.

3. Compute $\mathbf{G}^{(2)}((\eta, \omega)_\tau)$ by applying $f_{g,\tau}^S$ on $g_2^{\text{GSL}}((\eta, \omega)_\tau)$. The padded zeros in $\mathbf{r}^{\text{GSL}}$ are finally mapped to the inserted virtual atom. Hence, the zero-padding of $\mathbf{r}^{\text{GSL}}$ can be easily
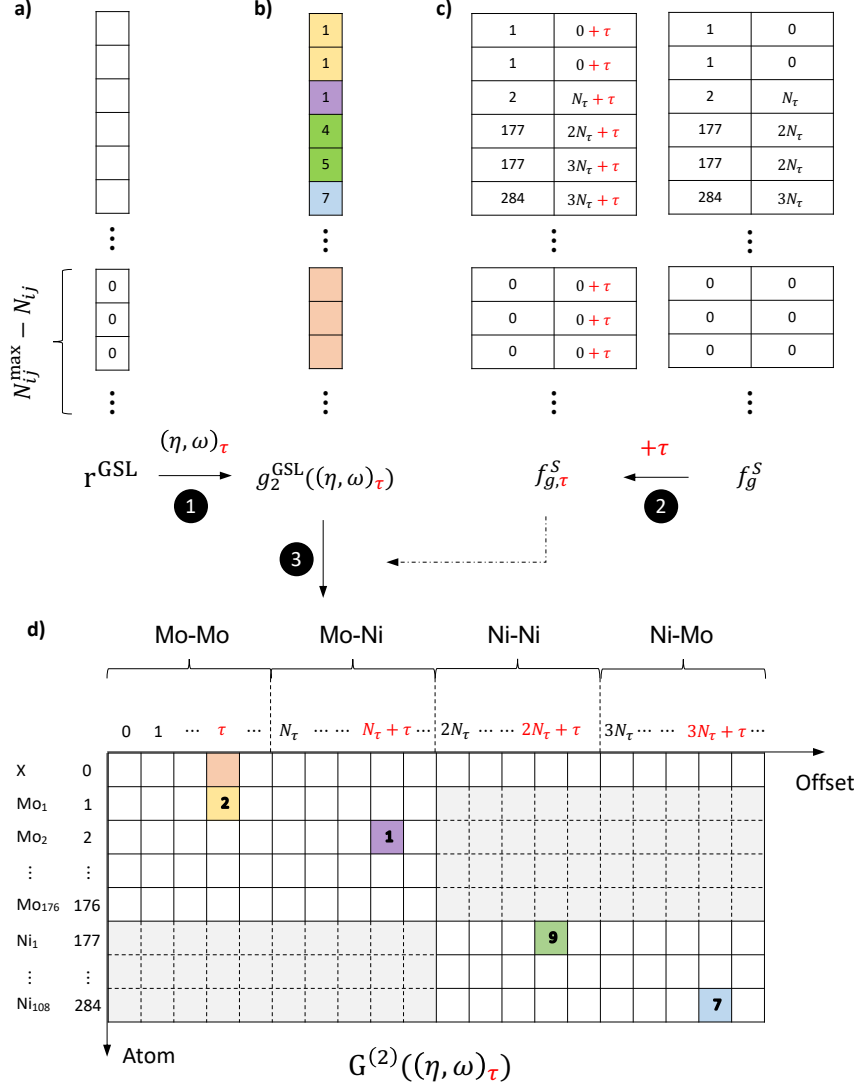
10

Figure 6: The calculation of $\mathbf{G}^{(2)}((\eta,\omega)_\tau)$ from $\mathbf{r}^{\text{GSL}}$.

separated and elinimated (just remove the first row of $\mathbf{G}^{(2)}$). That's why TensorAlloy can use arbitrary number of structures without any stoichiometry restriction to do batch training.

The mapping scheme f_v^S can be directly achieved using routine *tf.scatter_nd* implemented by TensorFlow. The calculation of the base mapping array f_g^S is implemented in Appendix(E). f_g^S is also cacheable. The calculation of $\mathbf{G}^{(2)}((\eta,\omega)_\tau)$ is implemented in method *get_g2_op_for_tau* of class *SymmetryFunction* in Appendix(G).

11

The workflow for the batch training phase is almost identical to the prediction phase described above. Meanwhile, there are some noticable diiferences:

1. Most of the variables ($\mathbf{r}^{\text{GSL}}$, $\mathbf{i}^{\text{GSL}}$, $\mathbf{R}^{\text{GSL}}$, etc.) have one more dimension. For example, $\mathbf{R}^{\text{GSL}}$ should be an array of shape $[N_b, N_{ij}^{\max}, 3]$. Here N_b represents the batch size.

2. The atomic descriptors $\mathbf{G}^{(2)}$ becomes a 3D array of shape $[N_b, N^{\text{vap}}, (N_{\text{element}})^2 \cdot N_\tau]$.

3. The base mapping f_g^S becomes a matrix of shape $[N_{ij}^{\max}, 3]$ in the batch training phase. The newly inserted first column —representing the batch indices —is **not cacheable** because structures are selected randomly to form a batch. Thus, the first column should be generated runtimely.

4. In the training phase, N^{vap} is a constant determined before training. In the contrast, N^{vap} should be a dynamic tensor (or a *tf.Placeholder* technically) in the prediction phase. Its value shall be runtimely determined according to the input structure.

5. In the training phase, the reference (or dft) atomic forces should be transformed to GSL arrays before computing the loss contribution. The NN-derived forces $\mathbf{F}^{\text{NN}}$ are indeed GSL forces:

$$\mathbf{F}^{\text{NN}} = -\frac{\partial E}{\partial \mathbf{R}^{\text{GSL}}} \tag{24}$$

Hence, in the prediction phase, a reverse transformation should be applied to obtain local $\mathbf{F}$.

The training phase is implemented in *BatchSymmetryFunction* which inherits most of methods from its parent class *SymmetryFunction*. The dynamic batching scheme is implemented in method *get_v2g_map_batch_indexing_matrix*. The method *get_g_shape* will return a fixed array instead. The function *map_gsl_array_to_local* of *VirtualAtomMap* is used to do the reverse mapping.

3.5. Angular descriptors

The same algorithm can be applied to compute angular symmetry function descriptors. The triple list shall be constructed from the neighbor list (Fig 3) and $N_{ij}^{\max}$ shall be replaced by $N_{ijk}^{\max}$. Typically $N_{ijk}^{\max} \gg N_{ij}^{\max}$.

Appendix(F) demonstrates how to compute the base mapping array. The calculation of $\mathbf{G}^{(4)}(\beta, \gamma, \zeta)_\tau$ is implemented in method *get_g4_op_for_tau* of class *SymmetryFunction* in Appendix(G).

3.6. Min-max normalization

Raw values of $\mathbf{G}^{(2)}$ and $\mathbf{G}^{(4)}$ may range from zero to several hundreds. So a min-max normalization routine is recommended. For each column $\mathbf{G}(:, \tau)$ where $0 \le \tau < N_\tau$, we just normalize its values to range $[0, 1]$:

$$\mathbf{G}(:, \tau) = \frac{\mathbf{G}(:, \tau) - \min(\mathbf{G}(:, \tau))}{\max(\mathbf{G}(:, \tau)) - \min(\mathbf{G}(:, \tau))} \tag{25}$$

where $\min(\mathbf{G}(:, \tau))$ and $\max(\mathbf{G}(:, \tau))$ should be determined in the training phase and remain constant in the prediction phase.

3.7. The residual model

To fit the total energy, we slightly modified the total energy expression of Equation 1:

$$E^{total} = E^{residual} + E^{static}$$
$$= \sum_{\text{el}} \mathbf{NN}_{el}(\mathbf{G}_{\text{el}}) + \sum_{\text{el}} n_{el} E_{el} \tag{26}$$

where $\{E_{el}\}$ is a set of *trainable* scalar variables representing the *static* energy of each type of element[13]. The NN in Equation 26 just describes the atomistic interactions (the *residual* energy). The introduction of E^{static} can significantly limit value range of NN outputs, leading to faster convergence speed and higher training stability (Fig 7c). The initial $\{E_{el}\}$ are calculated by solving the linear system $Ax = b$ where A is a $N_{data} \times N_{\text{element}}$ matrix and b is a vector of length N_{data}. N_{data} is the number of training examples. $A(i, j)$ is the number of j-th element in structure i and $b(i)$ is the corresponding total energy.

In the training phase, the atomic descriptors array $\mathbf{G}^{(2)}$ is a 3D array because of the structure-based batching scheme. Thus, it's necessarily to use convolutional neural networks (CNNs) with 1x1 kernels[13]. The traditional feed-forward neural networks with an additional atom-to-structure indexing[19, 17, 18, 35, 39] are mathematically equivalent to CNNs with 1x1 kernels. However, using CNNs can make the calculations of the *automatically-differentiated per-structure* $\partial E / \partial \mathbf{R}$ and $\partial E / \partial \mathbf{h}$ much easier.

To train the model, we use the following root mean-squared error (RMSE) total loss function:

$$\mathbf{Loss} = \sqrt{\frac{1}{N_b} \sum_{i=1}^{N_b} \left(E_i - E_i^{\text{dft}} \right)^2}$$
$$+ \chi_{\text{f}} \sqrt{\frac{1}{3N_b N^{\text{vap}}} \sum_{i}^{N_b} \sum_{j}^{N^{\text{vap}}} \sum_{\alpha} \left(f_{ij\alpha} - f_{ij\alpha}^{\text{dft}} \right)^2}$$
$$+ \chi_{\text{s}} \sqrt{\frac{1}{6N_b} \sum_{i}^{N_b} \sum_{j}^{6} \left(\epsilon_j^{\text{voigt}} - \epsilon_j^{\text{voigt,dft}} \right)^2} \tag{27}$$

where N_b is the mini-batch size and χ_{f} and χ_{s} are weights of force and virial losses. In most cases, we set N_b to 50 or 100 and we use the ADAM[40] optimizer with exponentially-decayed learning rate to minimize the loss function. The default activation function is softplus:

$$\sigma(x) = \log(1 + e^x) \tag{28}$$

Softplus is a smooth approximation of the ReLU activation function. The kernel weights of all NNs are initialized with the Xvaier method[41] and kernel biases are initialized with zeros.

4. Results and Discussions

In this section we demonstrate two experiments of TensorAlloy. All GPU benchmark results are obtained on the same workstation with two Intel Xeon E5-2687v4 CPUs (18 cores @ 2.3 GHz per CPU) and one NVIDIA GTX 1080Ti GPU.
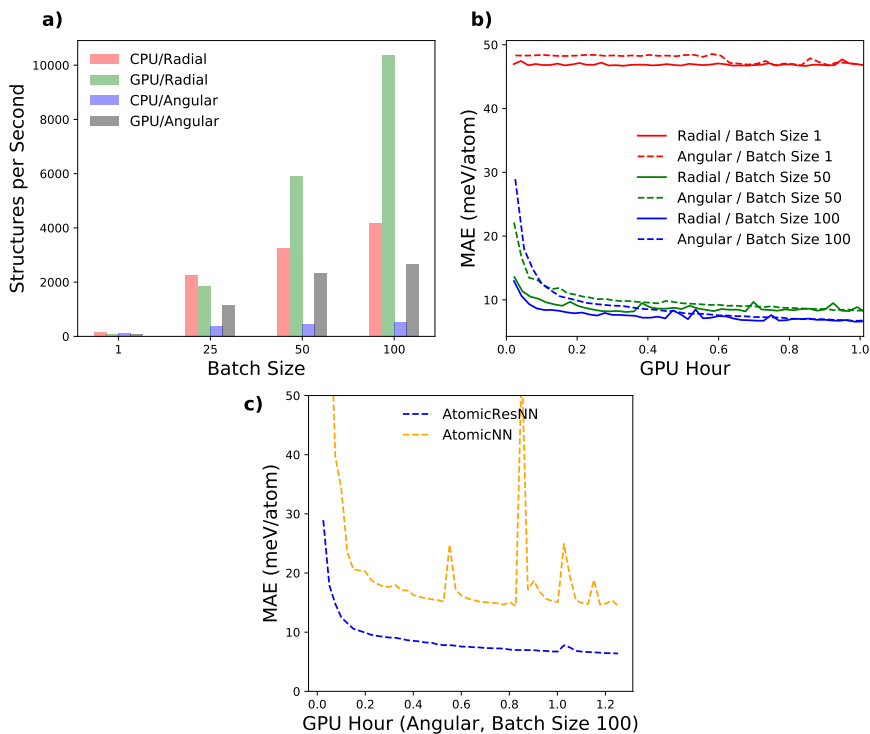
Figure 7: **a)** The curves of training speed (structures per second) vs batch sizes. **b)** The curves of test MAE (meV/atom) vs training time (GPU hour) using different settings. **c)** The curves of test MAE (meV/atom) vs NN models.

4.1. QM7

QM7[42, 43] is a publicly available benchmark dataset calculated at the DFT level. The QM7 dataset contains 7165 stable organic molecules (C, H, N, O, S) with 176 unique stoichiometries. The total energies range from -95 eV to -17 eV and the structure sizes range from 5 to 23. 1000 structures were randomly selected as test set before training.

Figure 7 demonstrates the performances of TensorAlloy on QM7 dataset. In this figure, 'Radial' means only radial symmetry functions (Equation 7) are used and 'Angular' indicates both radial and angular symmetry functions are used. The cutoff radius is 6.5 Å. The corresponding $N_{ij}^{\max}$ and $N_{ijk}^{\max}$ are 506 and 5313, respectively. Values of η for radial symmetry functions are 0.1, 0.5, 1, 2, 4, 8, 12, 16, 20, 40 and β (0.1, 0.5), γ (1, -1) and ζ (1, 4) are used for angular functions. ω is fixed to 0. The initial learning rate is 0.01. Learning rate decay is disabled for the following tests. Min-max normalization is enabled. Each atomistic neural network has two hidden layers with 64 and 32 neurons. The force and stress losses of Equation 27 are disabled for this experiment.

Figure 7a compares the training speed (number of processed structures per second) with different batch sizes (number of structures per step). It shows that CPU perfers fewer descriptors

14

(radial only) and smallber batch size while GPU is suitable for larger batch size and more compli-cated descriptors (radial + angular). Figure 7b shows the curves of mean absolute errors (MAEs, meV/atom) on the test set. This figure clearly illustrate another benefit of using larger batch size: the trainings can be much faster. For the best case (batch size 100, angular symmetry functions included), the test MAE will reach 6 meV/atom (1.8 kcal/mol per structure) in just one GPU hour on our workstation.

Figure 7c compares out residual model (Equation 26) with traditional ANN model (Equation 1). The proposed residual model has a much faster convergence rate and better stability. One exaplanation is that the *static* part acts as a normalization function. By introducing the *static* term, the output values of ANNs are much closer to the ideal output range (-1, 1) of neural networks.

4.2. Ni-Mo

SNAP/Ni-Mo[16, 12] is a publicly available dataset built by Shyue Ping Ong and co-workers. This dataset has 3971 Ni-Mo solids, including 461 pure Ni structures and 284 pure Mo structures. All DFT calculations were done by VASP[44] using the PBE[45] functional within the projector angumented-wave (PAW)[46] approach.

In this experiment, we trained three different models:

1. **NN**(Ni): this model uses 400 Ni structures for training and 61 for evaluation. The loss function only includes energy and force contributions.
2. **NN**(Mo): this model uses 250 Mo structures for training and 34 for evaluation. The loss function includes all three (energy, force, stress) types of contributions.
3. **NN**(Mo-Ni): this model uses 3673 structures for training and 300 for evaluation. The loss function includes all three types of contributions.

The cutoff radius is set to 6.5 Å. Only radial symmetry functions are used to compute atomic descriptors. The selected η are 0.1, 0.5, 1, 2, 4, 8, 12, 16, 20, 40 and ω are 0.0, 3.0. The hidden layer sizes are 128, 64, 32. The activation function is softplus. The learning rate starts from 0.01 and it will decay exponentially with rate 0.95 for every 3000 steps.

Binary Mo-Ni model			
Subset	Energy (meV/atom)	Force (eV/Å)	Stress (GPa)
Mo	16.5 (16.2)	0.28 (0.29)	0.75
Ni	4.5 (7.9)	0.07 (0.11)	0.83
Ni_4Mo	4.1 (4.0)	0.09 (0.14)	0.98
Ni_3Mo	4.5 (5.2)	0.11 (0.16)	1.19
Ni_{Mo}	12.9 (22.7)	0.09 (0.13)	0.34
Mo_{Ni}	12.9 (33.9)	0.12 (0.55)	0.45
Overall	10.8 (22.5)	0.11 (0.23)	0.59

Table 3: Comparion of the MAEs in predicted energies (mev/atom), forces (eV/Å) and stress (GPa) relative to DFT of each subset for the binary Mo-Ni model and the corresponding SNAP benchmarks (bracket)

Table 3 and 4 summarizes the energy, force and stress prediction performances of our trained models compared with their corresponding SNAP benchmarks. The original SNAP formal-ism contains both radial and angular interactions. However, in most cases, the radial-only TensorAlloy-trained models can significantly outperform corresponding SNAP models. We can

	Energy (meV/atom)		Force (eV/Å)		Stress (GPa)
Elementary Model	Mo	Ni	Mo	Ni	Mo
Mo	4.5 (13.2)		0.19 (0.25)		0.28 (0.87)
Ni		1.3 (1.2)		0.04 (0.05)	2.05

Table 4: Comparion of the MAEs in predicted energies (mev/atom), forces (eV/Å) and stress (GPa) relative to DFT for the two elementary models (Ni, Mo) and their corresponding SNAP benchmarks (bracket)

also notice that including virial stress in the total loss function can significantly reduce the stress prediction error. The virial stress (Equation 19) consists of two parts: the net force contribution $-F^T R$ and the partial force contribution $(\partial E/\partial \mathbf{h})^T \mathbf{h}$. The atomic forces used by the total loss equation 27 are net forces only but virial stress only depends on the partial forces (the force between two atoms). Compared with the binary **NN**(Mo-Ni) model, the elementary **NN**(Ni) model has lower net force error (0.04 eV/Åvs 0.07 eVÅ). However, the elementary model trained with energy and forces only has much larger stress MAE (2.05 GPa vs 0.83 GPa). These results clearly suggest that including virial stress in the total loss function is necessary for obtaining better virial stress accuracy.
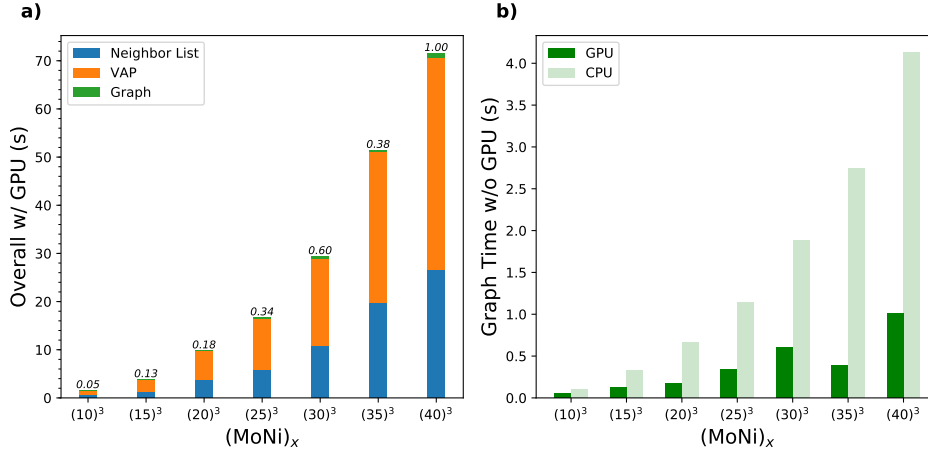

Figure 8: Benchmarks of the **NN**(Mo-Ni) model in the prediction phase. The test structures are $(MoNi)_x$ where $x = 10^3, 15^3, 20^3, 25^3, 30^3, 35^3, 40^3$. The left figure **a)** demonstrates the overall time and the right figure **b)** compares the 'Graph' time with/out GPU. Blue bars indicate the elapsed time (in seconds) for finding neighbors, orange bars denote the time for initializing VAP-GSL arrays and green bars and the numbers above represents the graph execution time (used for obtaining energy, forces and stress).

The speed of the prediction phase is also a crucial metric for measuring interaction potentials. Fig 8 summarizes the time distribution of the **NN**(Ni-Mo) model in the prediction phase on the GPU workstation. Here 'prediction' is defined as calculating energy, forces and stress tensor of an arbitrary *ase.Atoms* object. In these tests, the primitive structure MoNi is obtained by replacing one of the two bcc Mo atoms with a Ni atom. The test subjects $(MoNi))_x$ are just supercells of the base structure. We choose $x \in [10^3, 15^3, 20^3, 25^3, 30^3, 35^3, 40^3]$ as a typical molecular dynamics simulation for studying alloy properties needs at least thousands of atoms. The elasped time is splitted to three parts: 'Neighbor' (blue) indicates the execution time of the

neighbor_list routine of ASE for finding local neighbors ((**1**) of Fig 3), 'VAP' (orange) denotes the time to construct VAP-GSL arrays ((**2**) of Fig 3) and 'Graph' (green bars and the numbers above) represents the time of getting energy, forces and stress tensor by executing the computation graph. The smallest subject (2000 atoms) needs 1.6 seconds and the largest system (128000 atoms) requires 71.6 seconds on the workstation. Most of the time are spent on the Python-based single-thread 'Neighbor' and 'VAP' routines —which may be greatly optimized by utilizing efficient C/C++/Fortran codes (e.g. Lammps). For the 'Graph' part, the execution time can be as small as 1 second (with GPU) or 4 seconds (without GPU) for the 128000-atoms structure. According to these tests, it's fairly practical to use TensorAlloy-trained symmetry function interaction potential on studying large alloy systems.
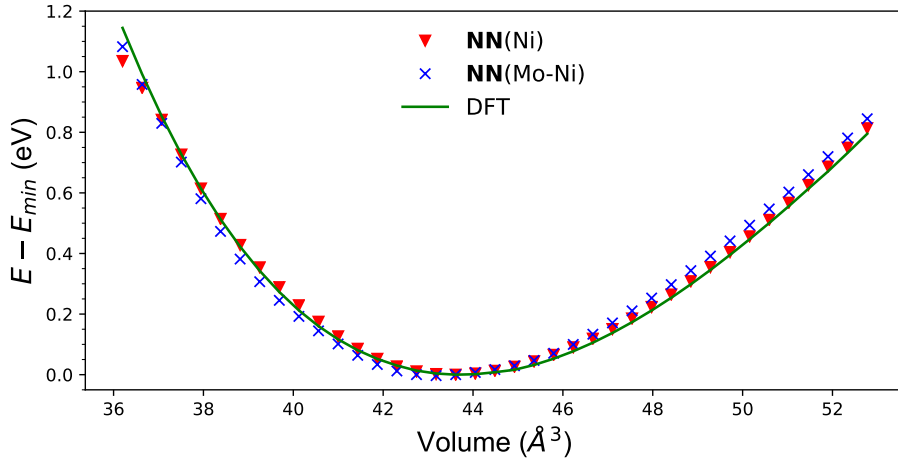

Figure 9: The energy vs volume curves of fcc Ni for the DFT, Ni and Ni-Mo models.

To further validate our models, we also calculate the energy-volume curves of a conventional fcc Ni cell using **NN**(Ni) and **NN**(Mo-Ni) models. The results are plotted in Fig 9. Both curves overlap the DFT curve very well in the range of -17% to 21% from the equilibrium volume. The surface energy tests, as shown in Fig 10, also proves the accuracy of TensorAlloy-optimized models. PyMatGen[47, 48] is used to generate these surface slabs.

5. Conclusions

In this work, we introduced our virtual atom approach and a smart way of constructing symmetry function based atomistic neural networks. With the virtual atom approach, the calculations of the symmetry function descriptors can be implemented within TensorFlow. Thus, we can now build direct computation graph from atomic positions to total energy, making the technical barrier of calculating NN-derived atomic forces and virial stress neglectable. Hence, not only energies and forces, but also virial stress, can be used to train atomistic neural networks. Our experiment also suggests that including virial stress in the total loss function can significantly improve the accuracy of predicting stress. All the new algorithms are implemented in our open-source Python program TensorAlloy.
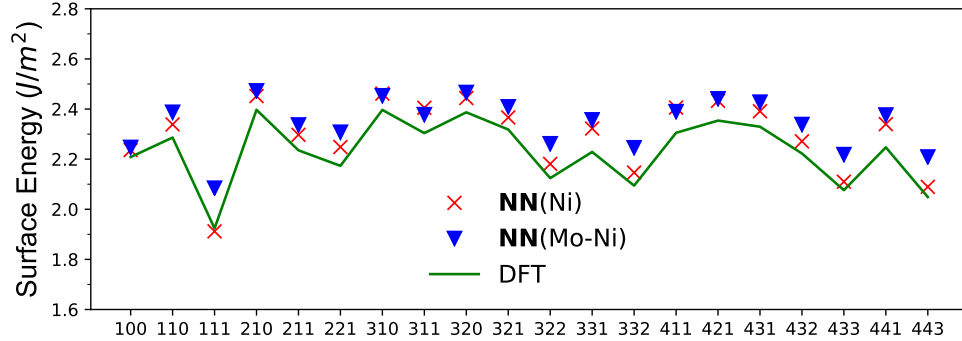
Figure 10: Surface formation energies (J/m^2) of different Ni surfaces calculated by DFT, Ni and Ni-Mo models

Acknowledgments

References

[1] M. S. Daw, M. I. Baskes, Semiempirical, quantum mechanical calculation of hydrogen embrittlement in metals, Phys. Rev. Lett 50 (17) (1983) 1285.

[2] M. S. Daw, M. I. Baskes, Embedded-atom method: Derivation and application to impurities, surfaces and other defects in metals, Phys. Rev. B 29 (12) (1984) 6443.

[3] M. I. Baskes, Modified embedded-atom potentials for cubic materials and impurities, Phys. Rev. B 46 (5) (1992) 2727–2742.

[4] X. W. Zhou, R. A. Johnson, H. N. G. Wadley, Misfit-energy-increasing dislocations in vapor-deposited cofe/nife multilayers, Phys. Rev. B 69 (14) (2004). `doi:10.1103/PhysRevB.69.144113`.

[5] B. Jelinek, S. Groh, M. F. Horstemeyer, J. Houze, S. G. Kim, G. J. Wagner, A. Moitra, M. I. Baskes, Modified embedded atom method potential for al, si, mg, cu, and fe alloys, Phys. Rev. B 85 (24) (2012). `doi:10.1103/PhysRevB.85.245102`.

[6] M. I. Baskes, R. A. Johnson, Modified embedded atom potentials for hcp metals, Modelling Simul. Mater. Sci. Eng. 2 (1994) 147–163.

[7] M. I. Baskes, Modified embedded-atom potentials for cubic materials and impurities, Phys. Rev. B 46 (5) (1992) 2727–2742.

[8] B.-J. Lee, J.-H. Shim, M. I. Baskes, Semiempirical atomic potentials for the fcc metals cu, ag, au, ni, pd, pt, al, and pb based on first and second nearest-neighbor modified embedded atom method, Phys. Rev. B 68 (14) (2003). `doi:10.1103/PhysRevB.68.144112`.

[9] Y. Mishin, A. Y. Lozovoi, Angular-dependent interatomic potential for tantalum, Acta Mater. 54 (19) (2006) 5013–5026. `doi:10.1016/j.actamat.2006.06.034`.

[10] Y. Mishin, M. J. Mehl, D. A. Papaconstantopoulos, Phase stability in the fe–ni system: Investigation by first-principles calculations and atomistic simulations, Acta Mater. 53 (15) (2005) 4029–4041. `doi:10.1016/j.actamat.2005.05.001`.

[11] G. P. Purja Pun, K. A. Darling, L. J. Kecskes, Y. Mishin, Angular-dependent interatomic potential for the cu–ta system and its application to structural stability of nano-crystalline alloys, Acta Mater. 100 (2015) 377–391. `doi:10.1016/j.actamat.2015.08.052`.

[12] X. G. Li, C. Hu, C. Chen, Z. Deng, J. Luo, S. P. Ong, Quantum-accurate spectral neighbor analysis potential models for ni-mo binary alloys and fcc metals, Phys. Rev. B. 98 (2018) 094104. `doi:10.1103/PhysRevB.98.094104`.

[13] X. Chen, M. S. Jorgensen, J. Li, B. Hammer, Atomic energies from a convolutional neural network, J. Chem. Theory Comput. 14 (7) (2018) 3933–3942. `doi:10.1021/acs.jctc.8b00149`.
URL `https://www.ncbi.nlm.nih.gov/pubmed/29812930`

[14] K. T. Schutt, H. E. Sauceda, P. J. Kindermans, A. Tkatchenko, K. R. Muller, Schnet - a deep learning architecture for molecules and materials, J. Chem. Phys 148 (24) (2018) 241722. `doi:10.1063/1.5019779`.
URL `https://www.ncbi.nlm.nih.gov/pubmed/29960322`

[15] K. T. Schutt, F. Arbabzadah, S. Chmiela, K. R. Muller, A. Tkatchenko, Quantum-chemical insights from deep tensor neural networks, Nat. Commun 8 (2017) 13890. `doi:10.1038/ncomms13890`.
URL `https://www.ncbi.nlm.nih.gov/pubmed/28067221`

[16] C. Chen, Z. Deng, R. Tran, H. Tang, I.-H. Chu, S. P. Ong, Accurate force field for molybdenum by machine learning large materials data, Phys. Rev. M 1 (4) (2017). `doi:10.1103/PhysRevMaterials.1.043603`.

[17] J. S. Smith, O. Isayev, A. E. Roitberg, Ani-1: an extensible neural network potential with dft accuracy at force field computational cost, Chem. Sci. 8 (4) (2017) 3192–3203. `doi:10.1039/c6sc05720a`.
URL `https://www.ncbi.nlm.nih.gov/pubmed/28507695`

[18] K. Yao, J. E. Herr, D. Toth, R. McKintyre, J. Parkhill, The tensormol-0.1 model chemistry: a neural network augmented with long-range physics, Chem. Sci. 9 (8) (2018) 2261–2269. `doi:10.1039/c7sc04934j`.

[19] J. Behler, M. Parrinello, Generalized neural-network representation of high-dimensional potential-energy surfaces, Phys. Rev. Lett 98 (14) (2007) 146401. `doi:10.1103/PhysRevLett.98.146401`.
URL `https://www.ncbi.nlm.nih.gov/pubmed/17501293`

[20] J. Behler, Atom-centered symmetry functions for constructing high-dimensional neural network potentials, J. Chem. Phys 134 (7) (2011) 074106. `doi:10.1063/1.3553717`.
URL `https://www.ncbi.nlm.nih.gov/pubmed/21341827`

[21] J. Behler, Representing potential energy surfaces by high-dimensional neural network potentials, J. Phys. Condens. Matter 26 (18) (2014) 183001. `doi:10.1088/0953-8984/26/18/183001`.
URL `https://www.ncbi.nlm.nih.gov/pubmed/24758952`

[22] J. Behler, Neural network potential-energy surfaces in chemistry: a tool for large-scale simulations, Phys. Chem. Chem. Phys 13 (2011) 17930–17955. `doi:0.1039/c1cp21668f`.

[23] J. Behler, Constructing high-dimensional neural network potentials: A tutorial review, Int. J. Quantum Chem. 115 (16) (2015) 1032–1050. `doi:10.1002/qua.24890`.

[24] S.-D. Huang, C. Shang, X.-J. Zhang, Z.-P. Liu, Material discovery by combining stochastic surface walking global optimization with a neural network, Chem. Sci. 8 (9) (2017) 6327–6337. `doi:10.1039/c7sc01459g`.

[25] S. Hajinazar, J. Shao, A. N. Kolmogorov, Stratified construction of neural network based interatomic models for multicomponent materials, Phys. Rev. B 95 (1) (2017). `doi:10.1103/PhysRevB.95.014114`.

[26] B. Onat, E. D. Cubuk, B. D. Malone, E. Kaxiras, Implanted neural network potentials: Application to li-si alloys, Phys. Rev. B 97 (9) (2018). `doi:10.1103/PhysRevB.97.094106`.

[27] R. Kobayashi, D. Giofré, T. Junge, M. Ceriotti, W. A. Curtin, Neural network potential for al-mg-si alloys, Phys. Rev. M 1 (5) (2017). `doi:10.1103/PhysRevMaterials.1.053604`.

[28] A. Khorshidi, A. A. Peterson, Amp: A modular approach to machine learning in atomistic simulations, Comput. Phys. Commun 207 (2016) 310–324. `doi:10.1016/j.cpc.2016.05.010`.

[29] E. L. Kolsbjerg, A. A. Peterson, B. Hammer, Neural-network-enhanced evolutionary algorithm applied to supported metal nanoparticles, Phys. Rev. B 97 (19) (2018). `doi:10.1103/PhysRevB.97.195424`.

[30] A. A. Peterson, Acceleration of saddle-point searches with machine learning, J. Chem. Phys 145 (2016). `doi:0.1063/1.4960708`.

[31] M. Abadi, P. Barham, J. Chen, Z. Chen, A. Davis, J. Dean, M. Devin, S. Ghemawat, G. Irving, M. Isard, M. Kudlur, J. Levenberg, R. Monga, S. Moore, D. G. Murray, B. Steiner, P. Tucker, V. Vasudevan, P. Warden, M. Wicke, Y. Yu, X. Zheng, Tensorflow: A system for large-scale machine learning, in: 12th USENIX Symposium on Operating Systems Design and Implementation (OSDI 16), USENIX Association, Savannah, GA, 2016, pp. 265–283.
URL `https://www.usenix.org/conference/osdi16/technical-sessions/presentation/abadi`

[32] A. Paszke, S. Gross, S. Chintala, G. Chanan, E. Yang, Z. DeVito, Z. Lin, A. Desmaison, L. Antiga, A. Lerer, Automatic differentiation in pytorch, in: NIPS-W, 2017.

[33] T. Chen, M. Li, Y. Li, M. Lin, N. Wang, M. Wang, T. Xiao, B. Xu, C. Zhang, Z. Zhang, MXNet: A Flexible and Efficient Machine Learning Library for Heterogeneous Distributed Systems, arXiv e-prints (2015) arXiv:1512.01274`arXiv:1512.01274`.

[34] A. P. Thompson, S. J. Plimpton, W. Mattson, General formulation of pressure and stress tensor for arbitrary many-body interaction potentials under periodic boundary conditions, J. Chem. Phys 131 (15) (2009) 154107. `doi:10.1063/1.3245303`.
URL `https://www.ncbi.nlm.nih.gov/pubmed/20568847`

[35] L. Zhang, J. Han, H. Wang, R. Car, W. E, Deep potential molecular dynamics: A scalable model with the accuracy of quantum mechanics, Phys. Rev. Lett. 120 (2018) 143001. `doi:10.1103/PhysRevLett.120.143001`.
URL `https://link.aps.org/doi/10.1103/PhysRevLett.120.143001`

[36] L. Zhang, H. Wang, W. E, Reinforced dynamics for enhanced sampling in large atomic and molecular systems, J. Chem. Phys 148 (12) (2018) 124113. `doi:10.1063/1.5019675`.

[37] H. Wang, L. Zhang, J. Han, W. E, Deepmd-kit: A deep learning package for many-body potential energy representation and molecular dynamics, Comput. Phys. Commun 228 (2018) 178 – 184. `doi:https://doi.org/10.1016/j.cpc.2018.03.016`.
URL `http://www.sciencedirect.com/science/article/pii/S0010465518300882`

[38] A. H. Larsen, J. J. Mortensen, J. Blomqvist, I. E. Castelli, R. Christensen, M. Dułak, J. Friis, M. N. Groves, B. Hammer, C. Hargus, E. D. Hermes, P. C. Jennings, P. B. Jensen, J. Kermode, J. R. Kitchin, E. L. Kolsbjerg, J. Kubal, K. Kaasbjerg, S. Lysgaard, J. B. Maronsson, T. Maxson, T. Olsen, L. Pastewka, A. Peterson, C. Rostgaard, J. Schiøtz, O. Schütt, M. Strange, K. S. Thygesen, T. Vegge, L. Vilhelmsen, M. Walter, Z. Zeng, K. W. Jacobsen, The atomic simulation environment—a python library for working with atoms, Journal of Physics: Condensed Matter 29 (27) (2017) 273002. `doi:10.1088/1361-648x/aa680e`.
URL `https://doi.org/10.1088%2F1361-648x%2Faa680e`

[39] K. Yao, J. E. Herr, S. N. Brown, J. Parkhill, Intrinsic bond energies from a bonds-in-molecules neural network, J. Phys. Chem. Lett 8 (12) (2017) 2689–2694. `doi:10.1021/acs.jpclett.7b01072`.
URL `https://www.ncbi.nlm.nih.gov/pubmed/28573865`

[40] D. P. Kingma, J. Ba, Adam: A method for stochastic optimization, CoRR abs/1412.6980 (2014). `arXiv:1412.6980`.
URL `http://arxiv.org/abs/1412.6980`

[41] X. Glorot, Y. Bengio, Understanding the difficulty of training deep feedforward neural networks, in: Y. W. Teh, M. Titterington (Eds.), Proceedings of the Thirteenth International Conference on Artificial Intelligence and Statistics, Vol. 9 of Proceedings of Machine Learning Research, PMLR, Chia Laguna Resort, Sardinia, Italy, 2010, pp. 249–256.
URL `http://proceedings.mlr.press/v9/glorot10a.html`

[42] L. C. Blum, J.-L. Reymond, 970 million druglike small molecules for virtual screening in the chemical universe database gdb-13, J. Am. Chem. Soc 131 (2009) 8732–8733. `doi:10.1021/ja902302h`.

[43] M. Rupp, A. Tkatchenko, K. R. Muller, O. A. von Lilienfeld, Fast and accurate modeling of molecular atomization energies with machine learning, Phys. Rev. Lett 108 (5) (2012) 058301. `doi:10.1103/PhysRevLett.108.058301`.
URL `https://www.ncbi.nlm.nih.gov/pubmed/22400967`

[44] G. Kresse, J. Furthmüller, Efficient iterative schemes for ab initio total-energy calculations using a plane-wave basis set, Phys. Rev. B 54 (1996) 11169–11186. `doi:10.1103/PhysRevB.54.11169`.
URL `https://link.aps.org/doi/10.1103/PhysRevB.54.11169`

[45] J. P. Perdew, K. Burke, M. Ernzerhof, Generalized gradient approximation made simple, Phys. Rev. Lett 77 (18) (1996) 3865–3868.
URL `https://link.aps.org/doi/10.1103/PhysRevLett.77.3865`

[46] P. E. Blöchl, Projector augmented-wave method, Phys. Rev. B 50 (1994) 17953–17979. `doi:10.1103/PhysRevB.50.17953`.
URL `https://link.aps.org/doi/10.1103/PhysRevB.50.17953`

[47] S. P. Ong, W. D. Richards, A. Jain, G. Hautier, M. Kocher, S. Cholia, D. Gunter, V. L. Chevrier, K. A. Persson, G. Ceder, Python materials genomics (pymatgen): A robust, open-source python library for materials analysis, Comput. Mater. Sci 68 (2013) 314–319. `doi:https://doi.org/10.1016/j.commatsci.2012.10.028`.
URL `http://www.sciencedirect.com/science/article/pii/S0927025612006295`

[48] W. Sun, G. Ceder, Efficient creation and convergence of surface slabs, Surf. Sci 617 (2013) 53–59. `doi:10.1016/j.susc.2013.05.016`.

Appendix

5.1. Derivation and implementation of the virial stress equation

According to Equation 6 and Equation 5, Equation 4 can be expanded:

$$
\begin{aligned}
r_{ij\mathbf{n}} &= \|\mathbf{r}_i^{(0)} - \mathbf{r}_j^{(0)} + \mathbf{n}^T \mathbf{h}\| \\
&= \left[\left(r_{j,x}^{(0)} - r_{i,x}^{(0)} + \sum_\alpha n_\alpha h_{\alpha x} \right)^2 + \left(r_{j,y}^{(0)} - r_{i,y}^{(0)} + \sum_\alpha n_\alpha h_{\alpha y} \right)^2 + \right. \\
&\quad \left. \left(r_{j,z}^{(0)} - r_{i,z}^{(0)} + \sum_\alpha n_\alpha h_{\alpha z} \right)^2 \right]^{\frac{1}{2}}
\end{aligned}
\tag{29}
$$

where $\alpha = x, y, z$. Thus, we can calculate the derivation of $r_{ij\mathbf{n}}$ with respect to $h_{\alpha\beta}$:

$$
\frac{\partial r_{ij\mathbf{n}}}{\partial h_{\alpha\beta}} = \frac{1}{r_{ij\mathbf{n}}} \cdot \Delta_{ij\mathbf{n}\beta} \cdot n_\alpha
\tag{30}
$$

$$
\Delta_{ij\mathbf{n}\beta} = r_{j,\beta}^{(0)} - r_{i,\beta}^{(0)} + \sum_\alpha n_\alpha h_{\alpha\beta}
\tag{31}
$$

Then we can derive $\partial E^{total} / \partial h_{\alpha\beta}$:

$$
\frac{\partial E^{total}}{\partial h_{\alpha\beta}} = \sum_i^N \sum_l^{N_G} \frac{\partial \mathbf{NN}_{el}(\mathbf{G}_i)}{\partial G_{il}} \cdot \frac{\partial G_{il}}{\partial h_{\alpha\beta}}
\tag{32}
$$

If G_{il} is a radial symmetry function:

$$
\frac{\partial G_{il}^{(2)}}{\partial h_{\alpha\beta}} = \sum_{j \neq i} \sum_{\mathbf{n}} \frac{\partial g_2}{\partial r_{ij\mathbf{n}}} \cdot \frac{1}{r_{ij\mathbf{n}}} \cdot \Delta_{ij\mathbf{n}\beta} \cdot n_\alpha
\tag{33}
$$

$$
\frac{\partial G_{il}^{(2)}}{\partial h_{\gamma\alpha}} \cdot h_{\gamma\beta} = \sum_{j \neq i} \sum_{\mathbf{n}} \frac{\partial g_2}{\partial r_{ij\mathbf{n}}} \cdot \frac{\Delta_{ij\mathbf{n}\alpha}}{r_{ij\mathbf{n}}} \cdot n_\gamma \cdot h_{\gamma\beta}
\tag{34}
$$

21

If G_{il} is an angular symmetry function:

$$\frac{\partial G_{il}^{(4)}}{\partial h_{\alpha\beta}} = \sum_{j,k\neq j,k\neq i} \sum_{\mathbf{n_1}} \sum_{\mathbf{n_2}} \sum_{\mathbf{n_3}} \left(\frac{\partial g_4}{\partial r_{ij\mathbf{n_1}}} \cdot \frac{\partial r_{ij\mathbf{n_1}}}{h_{\alpha\beta}} + \frac{\partial g_4}{\partial r_{ik\mathbf{n_2}}} \cdot \frac{\partial r_{ik\mathbf{n_2}}}{h_{\alpha\beta}} + \frac{\partial g_4}{\partial r_{jk\mathbf{n_3}}} \cdot \frac{\partial r_{jk\mathbf{n_3}}}{h_{\alpha\beta}} \right)$$

$$= \sum_{j,k\neq j,k\neq i} \sum_{\mathbf{n_1}} \sum_{\mathbf{n_2}} \sum_{\mathbf{n_3}} \frac{\partial g_4}{\partial r_{ij\mathbf{n_1}}} \cdot \frac{\Delta_{ij\mathbf{n_1}\beta}}{r_{ij\mathbf{n_1}}} \cdot n_{1,\alpha}$$

$$+ \sum_{j,k\neq j,k\neq i} \sum_{\mathbf{n_1}} \sum_{\mathbf{n_2}} \sum_{\mathbf{n_3}} \frac{\partial g_4}{\partial r_{ik\mathbf{n_2}}} \cdot \frac{\Delta_{ik\mathbf{n_2}\beta}}{r_{ik\mathbf{n_2}}} \cdot n_{2,\alpha}$$

$$+ \sum_{j,k\neq j,k\neq i} \sum_{\mathbf{n_1}} \sum_{\mathbf{n_2}} \sum_{\mathbf{n_3}} \frac{\partial g_4}{\partial r_{jk\mathbf{n_3}}} \cdot \frac{\Delta_{jk\mathbf{n_2}\beta}}{r_{jk\mathbf{n_3}}} \cdot n_{3,\alpha} \tag{35}$$

$$\frac{\partial G_{il}^{(4)}}{\partial h_{\gamma\alpha}} \cdot h_{\gamma\beta} = \sum_{j,k\neq j,k\neq i} \sum_{\mathbf{n_1}} \sum_{\mathbf{n_2}} \sum_{\mathbf{n_3}} \frac{\partial g_4}{\partial r_{ij\mathbf{n_1}}} \cdot \frac{\Delta_{ij\mathbf{n_1}\alpha}}{r_{ij\mathbf{n_1}}} \cdot n_{1,\gamma} \cdot h_{\gamma\beta}$$

$$+ \sum_{j,k\neq j,k\neq i} \sum_{\mathbf{n_1}} \sum_{\mathbf{n_2}} \sum_{\mathbf{n_3}} \frac{\partial g_4}{\partial r_{ik\mathbf{n_2}}} \cdot \frac{\Delta_{ik\mathbf{n_1}\alpha}}{r_{ik\mathbf{n_2}}} \cdot n_{2,\gamma} \cdot h_{\gamma\beta}$$

$$+ \sum_{j,k\neq j,k\neq i} \sum_{\mathbf{n_1}} \sum_{\mathbf{n_2}} \sum_{\mathbf{n_3}} \frac{\partial g_4}{\partial r_{jk\mathbf{n_3}}} \cdot \frac{\Delta_{jk\mathbf{n_1}\alpha}}{r_{jk\mathbf{n_3}}} \cdot n_{3,\gamma} \cdot h_{\gamma\beta} \tag{36}$$

Combining with Equation 32, 34 and 36, we can now start deriving the right part of Equation 19. To simplify the derivation, we just assume G_{il} represents a radial function:

$$\left(\left(\frac{\partial E^{total}}{\partial \mathbf{h}} \right)^T \mathbf{h} \right)_{\alpha\beta} = \sum_{\gamma} \frac{\partial E^{total}}{\partial h_{\gamma\alpha}} h_{\gamma\beta}$$

$$= \sum_{\gamma} \sum_{i}^{N} \sum_{l}^{N_G} \frac{\partial \mathbf{NN}_{el}(\mathbf{G}_i)}{\partial G_{il}} \cdot \sum_{j\neq i} \sum_{\mathbf{n}} \frac{\partial g_2}{\partial r_{ij\mathbf{n}}} \cdot \frac{\Delta_{ij\mathbf{n}\alpha}}{r_{ij\mathbf{n}}} \cdot n_{\gamma} h_{\gamma\beta}$$

$$= \sum_{i}^{N} \sum_{l}^{N_G} \sum_{j\neq i} \sum_{\mathbf{n}} \frac{\partial \mathbf{NN}_{el}(\mathbf{G}_i)}{\partial G_{il}} \cdot \frac{\partial g_2}{\partial r_{ij\mathbf{n}}} \cdot \frac{\Delta_{ij\mathbf{n}\alpha}}{r_{ij\mathbf{n}}} \sum_{\gamma} \cdot n_{\gamma} h_{\gamma\beta}$$

$$= - \sum_{i}^{N} \sum_{l}^{N_G} \sum_{j\neq i} \sum_{\mathbf{n}} f'_{ij\mathbf{n}\alpha} \sum_{\gamma} \cdot n_{\gamma} h_{\gamma\beta} \tag{37}$$

where $f'_{ij\mathbf{n}}$ is the partial force:

$$f'_{ij\mathbf{n}\alpha} = - \frac{\partial \mathbf{NN}_{el}(\mathbf{G}_i)}{\partial G_{il}} \cdot \frac{\partial g_2}{\partial r_{ij\mathbf{n}}} \cdot \frac{\Delta_{ij\mathbf{n}\alpha}}{r_{ij\mathbf{n}}} \tag{38}$$

If G_{il} is an angular symmetry function, we can also get a similar expression. Thus,

$$\left(\frac{\partial E^{total}}{\partial \mathbf{h}} \right)^T \mathbf{h} = - \left(\sum_{\mathbf{n}} \mathbf{h}^T \mathbf{n} \otimes \sum_{i=1}^{N} F'_{i\mathbf{n}} \right)^T \tag{39}$$

22

The left part of Equation 19 can be calculated with simple matrix multiplacation:

$$\sum_{i=1}^{N} \mathbf{r}_i^{(0)} \otimes f_i = R^T F \tag{40}$$

So finally we can derive the vectorized expression of virial stress:

$$\epsilon = -F^T R + \left(\frac{\partial E^{total}}{\partial \mathbf{h}}\right)^T \mathbf{h} \tag{41}$$

Now, the virial stress can be calculated with just a few lines of codes within arbitrary Machine Learning framework (TensorFlow, PyTorch, etc). The following codes are written in Python-3.7/TensorFlow-1.12, where *energy* and *volume* are scalar tensors, *cell* is a 3×3 tensor, R is a $N \times 3$ tensor and F (the total forces on these atoms) is also a $N \times 3$ tensor:

```
def get_virial_stress_tensor(energy, cell, volume, R, F):
    dEdh = tf.gradients(energy, cell, name='dEdh')[0]
    right = tf.matmul(tf.transpose(dEdh, name='dEdhT'), cell)
    left = tf.matmul(tf.transpose(F), R)
    virial = tf.add(tf.negative(left), right, name='virial')
    stress = tf.div(virial, volume, name='stress')
    return stress
```

5.2. Calculations of $N_{ij}^{\max}$ and $N_{ijk}^{\max}$

The following function returns N_{ij} and N_{ijk} of an ase.Atoms:

```python
def get_nij_and_nijk(atoms, rc, angular=False):
    ilist, jlist = neighbor_list('ij', atoms, cutoff=rc)
    nij = len(ilist)
    if angular:
        nl = {}
        for i, atomi in enumerate(ilist):
            if atomi not in nl:
                nl[atomi] = []
            nl[atomi].append(jlist[i])
        nijk = 0
        for atomi, nlist in nl.items():
            n = len(nlist)
            nijk += (n - 1 + 1) * (n - 1) // 2
    else:
        nijk = 0
    return nij, nijk
```

During the training phase, $N_{ij}^{\max}$ and $N_{ijk}^{\max}$ of a dataset (a collection of ase.Atoms objects) can be pre-computed with the following codes:

```python
nij_max = 0
nijk_max = 0
for atoms in dataset:
    nij, nijk = get_nij_and_nijk(atoms, rc, angular)
    nij_max = max(nij, nij_max)
    nijk_max = max(nijk, nijk_max)
```

5.3. Calculations of $N_{\text{element}}^{\max}$

The following function returns all $N_{\text{element}}^{\max}$ (e.g., $N_{\text{Ni}}^{\max}$) of a dataset:

```python
def get_max_occurs(dataset):
    from collections import Counter
    max_occurs = Counter()
    for atoms in dataset:
        c = Counter(atoms.get_chemical_symbols())
        for e, n in c.items():
            max_occurs[e] = max(n, max_occurs[e])
    return max_occurs
```

5.4. Implementation of the Virtual-Atom Map

The following class implements the core of the Virtual-Atom Approach. The argument *max_occurs* just represents the Global Symbol List (GSL). The positions and forces can be transformed to their GSL forms by using the function *map_to_gsl_array*.

```python
class VirtualAtomMap:
    REAL_ATOM_START = 1

    def __init__(self, max_occurs: Counter, symbols: List[str]):
        istart = VirtualAtomMap.REAL_ATOM_START
        self.max_occurs = max_occurs
        self.symbols = symbols
        self.max_vap_n_atoms = sum(max_occurs.values()) + istart
        elements = sorted(max_occurs.keys())
        offsets = np.cumsum([max_occurs[e] for e in elements])[:-1]
        offsets = np.insert(offsets, 0, 0)
        delta = Counter()
        index_map = {}
        mask = np.zeros(self.max_vap_n_atoms, dtype=bool)
        for i, symbol in enumerate(symbols):
            i_ele = elements.index(symbol)
            i_old = i + istart
            i_new = offsets[i_ele] + delta[symbol] + istart
            index_map[i_old] = i_new
            delta[symbol] += 1
            mask[i_new] = True
        reverse_map = {v: k - 1 for k, v in index_map.items()}
        index_map[0] = 0
        reverse_map[0] = -1
        self.atom_masks = mask
        self.index_map = index_map
        self.reverse_map = reverse_map
        self.splits = np.array([1, ] + [max_occurs[e] for e in elements])

    def map_array_to_gsl(self, array: np.ndarray):
        rank = np.ndim(array)
        if rank == 2:
            array = array[np.newaxis, ...]
        elif rank <= 1 or rank > 3:
            raise ValueError("The rank should be 2 or 3")
        if array.shape[1] == len(self.symbols):
            array = np.insert(
                array, 0, np.asarray(0, dtype=array.dtype), axis=1)
        else:
            shape = (array.shape[0], len(self.symbols), array.shape[2])
            raise ValueError(f"The shape should be {shape}")
        indices = []
        for i in range(self.max_vap_n_atoms):
            indices.append(
                self.reverse_map.get(i, -1) + self.REAL_ATOM_START)
        output = array[:, indices]
        if rank == 2:
```

```
            output = np.squeeze(output, axis=0)
        return output

    def reverse_map_gsl_to_local(self, array: np.ndarray):
        rank = np.ndim(array)
        if rank == 2:
            array = array[np.newaxis, ...]
        assert array.shape[1] == self.max_vap_n_atoms
        istart = self.REAL_ATOM_START
        indices = []
        for i in range(istart, istart + len(self.symbols)):
            indices.append(self.index_map[i])
        output = array[:, indices]
        if rank == 2:
            output = np.squeeze(output, axis=0)
        return output
```

5.5. Implementation of the g^2_{map}

This function shows the calculation of g^2_{map}. The returned dict is organized as follows:

- 'g2.v2g_map' : g^2_{map}

- 'g2.ilist' : $i^{(0)}_{+,\text{GSL}}$

- 'g2.jlist' : $j^{(0)}_{+,\text{GSL}}$

- 'g2.shift' : $\mathbf{n}_+$

$N^{\max}_{ij}$ should be provided in advance. *interactions* is a list of *string* representing the **ordered** interactions (e.g. ['NiNi','NiMo','MoMo','MoNi']). *offsets* is a list of integers marking the starting indices of the *interactions*. As an example, if N_η is 8, the *offsets* corresponding to ['NiNi','NiMo','MoMo','MoNi'] should be *[0, 8, 16, 24]*.

```
def get_g2_map(atoms: Atoms,
               rc: float,
               nij_max: int,
               interactions: list,
               vap: VirtualAtomMap,
               offsets: np.ndarray,
               for_prediction=False):
    if for_prediction:
        iaxis = 0
    else:
        iaxis = 1
    g2_map = np.zeros((nij_max, iaxis + 2), dtype=np.int32)
    tlist = np.zeros(nij_max, dtype=np.int32)
    symbols = atoms.get_chemical_symbols()
    tic = time.time()
```

```
ilist, jlist, n1 = neighbor_list('ijS', atoms, rc)
nij = len(ilist)
tlist.fill(0)
for i in range(nij):
    symboli = symbols[ilist[i]]
    symbolj = symbols[jlist[i]]
    tlist[i] = interactions.index('{}{}'.format(symboli, symbolj))
ilist = np.pad(ilist + 1, (0, nij_max - nij), 'constant')
jlist = np.pad(jlist + 1, (0, nij_max - nij), 'constant')
n1 = np.pad(n1, ((0, nij_max - nij), (0, 0)), 'constant')
n1 = n1.astype(np.float32)
for count in range(len(ilist)):
    if ilist[count] == 0:
        break
    ilist[count] = vap.index_map[ilist[count]]
    jlist[count] = vap.index_map[jlist[count]]
g2_map[:, iaxis + 0] = ilist
g2_map[:, iaxis + 1] = offsets[tlist]
return {"g2.v2g_map": g2_map, "g2.ilist": ilist, "g2.jlist": jlist,
        "g2.shift": n1}
```

5.6. Implementation of the g^4_{map}

The construction of g^4_{map} is similar to g^2_{map}. N^{max}_{ijk} should be provided in advance.

One must note that 'g2.ilist' contains GSL indices while the symbol list of the target *Atoms* is in local order. So the *reverse* mapping is necessary.

```
def get_g4_map(atoms: Atoms,
               g2_map: dict,
               interactions: list,
               offsets: np.ndarray,
               vap: VirtualAtomMap,
               nijk_max: int,
               for_prediction=True):
    if for_prediction:
        iaxis = 0
    else:
        iaxis = 1
    g4_map = np.zeros((nijk_max, iaxis + 2), dtype=np.int32)
    ijk = np.zeros((nijk_max, 3), dtype=np.int32)
    n1 = np.zeros((nijk_max, 3), dtype=np.float32)
    n2 = np.zeros((nijk_max, 3), dtype=np.float32)
    n3 = np.zeros((nijk_max, 3), dtype=np.float32)
    symbols = atoms.get_chemical_symbols()
    indices = {}
    vectors = {}
    for i, atom_gsl_i in enumerate(g2_map["g2.ilist"]):
        if atom_gsl_i == 0:
```

```
                break
        if atom_gsl_i not in indices:
            indices[atom_gsl_i] = []
            vectors[atom_gsl_i] = []
        indices[atom_gsl_i].append(g2_map["g2.jlist"][i])
        vectors[atom_gsl_i].append(g2_map["g2.shift"][i])
    count = 0
    for atom_gsl_i, nl in indices.items():
        atom_local_i = vap.reverse_map[atom_gsl_i]
        symboli = symbols[atom_local_i]
        prefix = '{}'.format(symboli)
        for j in range(len(nl)):
            atom_vap_j = nl[j]
            atom_local_j = vap.reverse_map[atom_vap_j]
            symbolj = symbols[atom_local_j]
            for k in range(j + 1, len(nl)):
                atom_vap_k = nl[k]
                atom_local_k = vap.reverse_map[atom_vap_k]
                symbolk = symbols[atom_local_k]
                interaction = '{}{}'.format(
                    prefix, ''.join(sorted([symbolj, symbolk])))
                ijk[count] = atom_gsl_i, atom_vap_j, atom_vap_k
                n1[count] = vectors[atom_gsl_i][j]
                n2[count] = vectors[atom_gsl_i][k]
                n3[count] = n2[count] - n1[count]
                index = interactions.index(interaction)
                g4_map[count, iaxis + 0] = atom_gsl_i
                g4_map[count, iaxis + 1] = offsets[index]
                count += 1
    return {"g4.v2g_map": g4_map,
            "g4.ij.ilist": ijk[:, 0], "g4.ij.jlist": ijk[:, 1],
            "g4.ik.ilist": ijk[:, 0], "g4.ik.klist": ijk[:, 2],
            "g4.jk.jlist": ijk[:, 1], "g4.jk.klist": ijk[:, 2],
            "g4.shift.ij": n1, "g4.shift.ik": n2, "g4.shift.jk": n3}
```

5.7. Compute the descriptors

Now we can implements the symmetry function descriptor. Here *SymmetryFunction* is the base class and *BatchSymmetryFunction* is its subclass for batch training.

The return value of the method *build_graph* is a dict and its keys are chemical elements and values are correspond atomic descriptors and atom masks. Taking the example of the Ni-Mo dataset with $r_c = 4.6$, batch size 10 and only 10 radial symmetry functions, the corresponding $N_{ij}^{\max}$, $N_{\mathrm{Ni}}^{\max}$ and $N_{\mathrm{Mo}}^{\max}$ are 108, 176 and 7200, respectively. Thus, the return dict should be:

- 'Mo': $(\mathbf{G}^{\mathrm{Mo}}, \delta^{\mathrm{Mo}})$

- 'Ni': $(\mathbf{G}^{\mathrm{Ni}}, \delta^{\mathrm{Ni}})$

where $\mathbf{G}^{\text{Mo}}$ is a float tensor of shape [10, 176, 40], δ^{Mo} is a float tensor of shape [10, 176], $\mathbf{G}^{\text{Ni}}$ is a float tensor of shape [10, 108, 40] and δ^{Ni} is a float tensor of shape [10, 108] during the training phase.

```python
class SymmetryFunction:
    gather_fn = staticmethod(tf.gather)

    def __init__(self, rc, elements, eta=np.array([0.05, 4, 20, 80]),
                 omega=np.array([0.0]), beta=np.array([0.005, ]),
                 gamma=np.array([1.0, -1.0]), zeta=np.array([1.0, 4.0]),
                 angular=True, periodic=True):
        all_kbody_terms, kbody_terms, elements = \
            get_kbody_terms(elements, angular=angular)
        ndim, kbody_sizes = compute_dimension(
            all_kbody_terms, len(eta), len(omega), len(beta), len(gamma),
            len(zeta))
        self.rc = rc
        self.all_kbody_terms = all_kbody_terms
        self.kbody_terms = kbody_terms
        self.elements = elements
        self.n_elements = len(elements)
        self.periodic = periodic
        self.angular = angular
        self.kbody_sizes = kbody_sizes
        self.ndim = ndim
        self.kbody_index = {
            kbody_term: self.all_kbody_terms.index(kbody_term)
            for kbody_term in self.all_kbody_terms}
        self.offsets = np.insert(np.cumsum(kbody_sizes), 0, 0)
        self.radial_indices_grid = ParameterGrid({
            'eta': np.arange(len(eta), dtype=int),
            'omega': np.arange(len(omega), dtype=int)})
        self.angular_indices_grid = ParameterGrid({
            'beta': np.arange(len(beta), dtype=int),
            'gamma': np.arange(len(gamma), dtype=int),
            'zeta': np.arange(len(zeta), dtype=int)})
        self.initial_values = {'eta': eta, 'omega': omega,
                               'gamma': gamma,
                               'beta': beta, 'zeta': zeta}

    @staticmethod
    def get_pbc_displacements(shift, cells, dtype=tf.float32):
        return tf.matmul(shift, cells, name='displacements')

    def get_rij(self, positions, cells, ilist, jlist, shift, name):
        with tf.name_scope(name):
            dtype = positions.dtype
```

```python
            Ri = self.gather_fn(positions, ilist, 'Ri')
            Rj = self.gather_fn(positions, jlist, 'Rj')
            Dij = tf.subtract(Rj, Ri, name='Dij')
            if self.periodic:
                pbc = self.get_pbc_displacements(shift, cells, dtype)
                Dij = tf.add(Dij, pbc, name='pbc')
            with tf.name_scope("safe_norm"):
                eps = tf.constant(1e-8, dtype=dtype, name='eps')
                rij = tf.sqrt(tf.reduce_sum(
                    tf.square(Dij, name='Dij2'), axis=-1) + eps)
                return rij, Dij

    def get_v2g_map(self, features: dict, prefix: str):
        return tf.identity(features[f"{prefix}.v2g_map"], name='v2g_map')

    @staticmethod
    def get_v2g_map_delta(tau):
        return tf.constant([0, tau], dtype=tf.int32, name='delta')

    def get_g_shape(self, features: dict):
        return [features['n_atoms_vap'], self.ndim]

    def get_g2_op_for_tau(self, shape, tau, r, rc2, fc_r, base_v2g_map):
        with tf.name_scope(f"Grid{tau}"):
            grid = self.radial_indices_grid[tau]
            etai = grid['eta']
            omegai = grid['omega']
            eta = tf.constant(self.initial_values['eta'][etai], r.dtype)
            omega = tf.constant(
                self.initial_values['omega'][omegai], r.dtype)
            delta = self.get_v2g_map_delta(tau)
            r2c = tf.math.truediv(tf.square(r - omega), rc2, name='r2c')
            v = tf.exp(-tf.multiply(eta, r2c, 'eta_r2c')) * fc_r
            v2g_map_tau = tf.add(base_v2g_map, delta, f'v2g_map_{tau}')
            return tf.scatter_nd(v2g_map_tau, v, shape, f"g{tau}")

    def get_g2_op(self, features: dict):
        with tf.variable_scope("G2"):
            r = self.get_rij(features['positions'],
                             features['cells'],
                             features['g2.ilist'],
                             features['g2.jlist'],
                             features['g2.shift'],
                             name='rij')[0]
            rc2 = tf.constant(self.rc**2, dtype=r.dtype, name='rc2')
            fc_r = cosine_cutoff(r, rc=self.rc, name='fc_r')
            base_v2g_map = self.get_v2g_map(features, prefix='g2')
```
30

```python
        shape = self.get_g_shape(features)
        values = []
        for tau in range(len(self.radial_indices_grid)):
            values.append(
                self.get_g2_op_for_tau(
                    shape, tau, r, rc2, fc_r, base_v2g_map))
        return tf.add_n(values, name='g')

def get_g4_op_for_tau(self, shape, tau: int, cos_theta, r2c, fc_r,
                      base_v2g_map):
    with tf.name_scope(f"Grid{tau}"):
        grid = self.angular_indices_grid[tau]
        betai = grid['beta']
        gammai = grid['gamma']
        zetai = grid['zeta']
        beta = tf.constant(
            self.initial_values['beta'][betai], r2c.dtype)
        gamma = tf.constant(
            self.initial_values['gamma'][gammai], r2c.dtype)
        zeta = tf.constant(
            self.initial_values['zeta'][zetai], r2c.dtype)
        delta = self.get_v2g_map_delta(tau)
        one = tf.constant(1.0, dtype=r2c.dtype, name='one')
        two = tf.constant(2.0, dtype=r2c.dtype, name='two')
        gt = tf.math.multiply(gamma, cos_theta, name='gt')
        gt1 = tf.add(gt, one, name='gt1')
        gt1z = tf.pow(gt1, zeta)
        z1 = tf.math.subtract(one, zeta, name='z1')
        z12 = tf.pow(two, z1)
        c = tf.math.multiply(gt1z, z12, name='c')
        v = tf.multiply(c * tf.exp(-beta * r2c), fc_r, f'v_{tau}')
        v2g_map_tau = tf.add(
            base_v2g_map, delta, name=f'v2g_map_{tau}')
        return tf.scatter_nd(v2g_map_tau, v, shape, f'g{tau}')

def get_g4_op(self, features: dict):
    with tf.variable_scope("G4"):
        rij = self.get_rij(features['positions'],
                           features['cells'],
                           features['g4.ij.ilist'],
                           features['g4.ij.jlist'],
                           features['g4.shift.ij'],
                           name='rij')[0]
        rik = self.get_rij(features['positions'],
                           features['cells'],
                           features['g4.ik.ilist'],
                           features['g4.ik.klist'],
```

31

```python
                            features['g4.shift.ik'],
                            name='rik')[0]
        rjk = self.get_rij(features['positions'],
                            features['cells'],
                            features['g4.jk.jlist'],
                            features['g4.jk.klist'],
                            features['g4.shift.jk'],
                            name='rjk')[0]
        rij2 = tf.square(rij, name='rij2')
        rik2 = tf.square(rik, name='rik2')
        rjk2 = tf.square(rjk, name='rjk2')
        rc2 = tf.constant(self.rc**2, dtype=rij.dtype, name='rc2')
        r2 = tf.add_n([rij2, rik2, rjk2], name='r2')
        r2c = tf.math.truediv(r2, rc2, name='r2_rc2')
        with tf.name_scope("CosTheta"):
            upper = tf.subtract(rij2 + rik2, rjk2, name='upper')
            lower = tf.multiply(2.0 * rij, rik, name='lower')
            cos_theta = tf.math.truediv(upper, lower, name='theta')
        with tf.name_scope("Cutoff"):
            fc_rij = cosine_cutoff(rij, rc=self.rc, name='fc_rij')
            fc_rik = cosine_cutoff(rik, rc=self.rc, name='fc_rik')
            fc_rjk = cosine_cutoff(rjk, rc=self.rc, name='fc_rjk')
            fc_r = tf.multiply(fc_rij, fc_rik * fc_rjk, 'fc_r')
        base_v2g_map = self.get_v2g_map(features, prefix='g4')
        shape = self.get_g_shape(features)
        values = []
        for tau in range(len(self.angular_indices_grid)):
            values.append(
                self.get_g4_op_for_tau(
                    shape, tau, cos_theta, r2c, fc_r, base_v2g_map))
        return tf.add_n(values, name='g')

    def get_row_split_sizes(self, features: dict):
        return features['row_splits']

    @staticmethod
    def get_row_split_axis():
        return 0

    def get_column_split_sizes(self):
        column_splits = {}
        for i, element in enumerate(self.elements):
            column_splits[element] = [len(self.elements), i]
        return column_splits

    @staticmethod
    def get_column_split_axis():
```

```python
            return 1

    def split_descriptors(self, descriptors, features: dict):
        with tf.name_scope("Split"):
            row_split_sizes = self.get_row_split_sizes(features)
            row_split_axis = self.get_row_split_axis()
            column_split_sizes = self.get_column_split_sizes()
            column_split_axis = self.get_column_split_axis()
            splits = tf.split(
                descriptors, row_split_sizes, axis=row_split_axis,
                name='rows')[1:]
            atom_masks = tf.split(
                features['atom_masks'], row_split_sizes,
                axis=row_split_axis,
                name='atom_masks')[1:]
            if len(self.elements) > 1:
                blocks = []
                for i in range(len(splits)):
                    element = self.elements[i]
                    size_splits, idx = column_split_sizes[element]
                    block = tf.split(splits[i],
                                     size_splits,
                                     axis=column_split_axis,
                                     name=f'{element}_block')[idx]
                    blocks.append(block)
            else:
                blocks = splits
            return dict(zip(self.elements, zip(blocks, atom_masks)))

    def build_graph(self, features: dict):
        with tf.variable_scope("Behler"):
            descriptors = self.get_g2_op(features)
            if self.angular:
                descriptors += self.get_g4_op(features)
        return self.split_descriptors(descriptors, features)


class BatchSymmetryFunction(SymmetryFunction):
    gather_fn = staticmethod(tf.batch_gather)

    def __init__(self, rc, max_occurs: Counter, nij_max: int,
                 nijk_max: int, batch_size: int,
                 eta=np.array([0.05, 4.0, 20.0, 80.0]),
                 omega=np.array([0.0]), beta=np.array([0.005, ]),
                 gamma=np.array([1.0, -1.0]), zeta=np.array([1.0, 4.0]),
                 angular=True, periodic=True):
        elements = sorted(list(max_occurs.keys()))
```

```python
        super(BatchSymmetryFunction, self).__init__(
            rc=rc, elements=elements, eta=eta, beta=beta, gamma=gamma,
            zeta=zeta, omega=omega, angular=angular, periodic=periodic)
        self._max_occurs = max_occurs
        self._max_n_atoms = sum(max_occurs.values())
        self._nij_max = nij_max
        self._nijk_max = nijk_max
        self._batch_size = batch_size

    @staticmethod
    def get_pbc_displacements(shift, cells, dtype=tf.float32):
        with tf.name_scope("Einsum"):
            shift = tf.convert_to_tensor(shift, dtype, name='shift')
            cells = tf.convert_to_tensor(cells, dtype, name='cells')
            return tf.einsum(
                'ijk,ikl->ijl', shift, cells, name='displacements')

    def get_g_shape(self, _):
        n_atoms_vap = self._max_n_atoms + 1
        return [self._batch_size, n_atoms_vap, self.ndim]

    def get_v2g_map_batch_indexing_matrix(self, prefix='g2'):
        if prefix == 'g2':
            ndim = self._nij_max
        else:
            ndim = self._nijk_max
        indexing_matrix = np.zeros(
            (self._batch_size, ndim, 3), dtype=np.int32)
        for i in range(self._batch_size):
            indexing_matrix[i] += [i, 0, 0]
        return indexing_matrix

    @staticmethod
    def get_v2g_map_delta(tau):
        return tf.constant([0, 0, tau], tf.int32, name='delta')

    def get_v2g_map(self, features: dict, prefix="g2"):
        indexing = self.get_v2g_map_batch_indexing_matrix(prefix=prefix)
        return tf.add(
            features[f"{prefix}.v2g_map"], indexing, name='v2g_map')

    def get_row_split_sizes(self, _):
        row_splits = [1, ]
        for i, element in enumerate(self.elements):
            row_splits.append(self._max_occurs[element])
        return row_splits
```

```python
@staticmethod
def get_row_split_axis():
    return 1

@staticmethod
def get_column_split_axis():
    return 2
```